



# Double-barrier Josephson structures as the novel elements for superconducting large-scale integrated circuits

M.Yu. Kupriyanov <sup>a</sup>, A. Brinkman <sup>b</sup>, A.A. Golubov <sup>b,\*</sup>, M. Siegel <sup>c</sup>, H. Rogalla <sup>b</sup>

<sup>a</sup> *Institute of Nuclear Physics, Moscow State University, 119899 GSP Moscow, Russian Federation*

<sup>b</sup> *Department of Applied Physics, University of Twente, P.O. Box 217, 7500 AE Enschede, The Netherlands*

<sup>c</sup> *Institute of Thin Films and Ion Technology, KFA-Juelich, D42425 Juelich, Germany*

Received 25 April 1999; received in revised form 9 July 1999; accepted 13 July 1999

---

## Abstract

An overview of the current status of different types of non-hysteretic Josephson junctions is given with emphasis on double-barrier structures. The results of theoretical work on double-barrier SIS'IS Josephson junctions (I is a tunnel barrier, S' is a thin film with  $T_{C'} < T_C$ ) are presented. The microscopic model for the supercurrent is developed for two cases: the S' interlayer in the clean and in the dirty limit. The model describes the cross-over from direct Josephson coupling of the external S electrodes to the regime of two serially connected SIS' junctions. We calculate the  $I_C R_N$  product as a function of the  $T_{C'}/T_C$  ratio, the interlayer thickness and the barrier strengths and compare the theory with experimental data for Nb/AIO<sub>x</sub>/Al/AIO<sub>x</sub>/Nb junctions. We argue that these junctions are very promising in rapid single flux quantum (RSFQ) and programmable voltage standard applications, since they are intrinsically shunted and have controllable interfaces. We formulate the requirements for materials and interface barriers in order to increase critical current densities and  $I_C R_N$  products in double-barrier junctions. © 1999 Elsevier Science B.V. All rights reserved.

*Keywords:* Double-barrier; Josephson structures; Integrated circuits

---

## 1. Introduction

The general tendency in the development of modern fabrication processes focuses on a further miniaturization of the basic elements of practical superconducting devices down to the nanometer scale. Simple estimations clearly show that in the case of Josephson junctions this tendency must be accompanied by the development of a technology based on concepts that differ from the existing solutions for the well known Nb/Al tunnel junction fabrication process [1].

To provide the required low error rate of rapid single flux quantum (RSFQ) devices [2], the critical current  $I_C$  should exceed approximately 500 times the effective noise current  $I_f$  of  $0.042T$  [K]. At helium temperatures  $T = 4.2$  K, this results in  $I_f = 0.1764 \mu\text{A}$  and, hence,  $I_C$  must be of the order of or larger than  $100 \mu\text{A}$ . Thus,

---

\* Corresponding author. Tel.: +31-53-489-3122; fax: +31-53-489-1099; E-mail: a.golubov@tn.utwente.nl

for junctions with an area  $S$  down to  $0.1 \times 0.1 \mu\text{m}^2$  the critical current density  $J_C = I_C/S$  should exceed  $103 \text{ kA/cm}^2$ . It seems to be impossible to achieve this value in the standard Nb/Al/AIO<sub>x</sub>Nb tunnel junction technology. It is also important that the current–voltage characteristic (CVC) of the Josephson junction should be close to the resistively shunted junction (RSJ) type 1 [2].

The new concept of a programmable voltage standard [3] also essentially employs junctions with a non-hysteretic CVC and a large current density. In contrast to classical designs of the voltage standard which considered a series array of Josephson junctions as a passive conductance–inductance (CL)-transmission line, which has to be pumped uniformly by external microwave irradiation, the new concept uses the active nature of Josephson junctions [4]. It has for the very first time been demonstrated in Ref. [4] that the external microwave field does not have to generate the propagating wave in the transmission line but that the Josephson array itself behaves as a complex of microwave generators which pump and synchronize each other. This allows a rapid selection of the desired voltage step just by applying the dc-bias current to the appropriate array section, provides greater stability against thermal fluctuations, greater output current and faster slew rate. Since it is not necessary anymore for the local oscillator to pump all of the junctions in the array, its power can be lower than in a classical voltage standard configuration. This fact and the extremely high stability of flux flow oscillators which has been demonstrated recently [5,6] (half-width  $\approx 1 \text{ Hz}$  at a frequency up to  $440 \text{ GHz}$ ) opens the way to fully integrated on-chip voltage standards in which both the oscillator (analogous flux flow or based on a RSFQ concept) and the series array of Josephson junctions are fabricated on one chip.

An increase in the critical current density of tunnel SIS Josephson junctions had been considered as one of the possible concepts for elements with non-hysteretic CVC but only recently [7] it has been demonstrated that this approach faces serious physical difficulties. A RSFQ divider which consisted of six to eight Josephson junctions with  $J_C$ s in the range of  $50\text{--}200 \text{ kA/cm}^2$  and a minimum junction size of  $0.25 \mu\text{m}^2$  has been fabricated and studied [7]. The circuits, based on externally shunted junctions with  $J_C = 50 \text{ kA/cm}^2$ , have been demonstrated to operate correctly at  $T = 1.8 \text{ K}$  and at frequencies higher than  $750 \text{ GHz}$ . The circuit with Josephson junctions having a further four times increase in  $J_C$  was not operational at these high frequencies. A measurable error signal was detected even at a lower frequency of  $520 \text{ GHz}$  and a temperature of  $1.8 \text{ K}$ . These instabilities were associated with the complex character of non-stationary processes in the junctions due to peculiarities on their CVC caused by multiple Andreev reflection (MAR) resonances.

Thus, in RSFQ devices based on Nb/Al/AIO<sub>x</sub>Nb tunnel junctions resistive shunts must be used not only for the suppression of the Stewart–McCumber parameter  $\beta_C = (2\pi(I_C R_{\text{sh}})^2 C_S)/(\phi_0 J_C)$  to a value of the order of unity, but also to avoid instabilities due to (MAR) resonances on CVC. Here,  $I_C$ ,  $R_{\text{sh}}$ , and  $C_S$  are the critical current, the effective shunt resistor, and the specific capacity of the junction, respectively,  $\phi_0$  is the flux quantum,  $\phi_0 = h/2e = 2.07 \times 10^{-15} \text{ Wb}$ . These shunts have geometrical sizes of the order of  $10\text{--}100 \mu\text{m}^2$  and some wiring must be used for their connection to the junctions. This makes the fabrication processes more complicated and increases the effective area of the junctions. Moreover, these shunts reduce the high-frequency performance of the circuits,  $f_C = I_C R_{\text{sh}}/\phi_0$  and cause a parasitic inductance parallel to the junction. This inductance increases with a decrease in the junction's area  $S$  and can lead to undesirable dynamic effects [2].

Thus, the transition from classical Nb/Al/AIO<sub>x</sub>Nb tunnel junctions to the intrinsically shunted SIS/IS structures or SNS weak links (N is a normal metal) seems to be very natural for the future development of basic elements for large-scale integrated superconducting circuits. We can raise the question, which type of Josephson junctions will be appropriate then for submicron superconducting devices? At the moment, there are three types of Josephson junctions with non-hysteretic CVC. They are

- Josephson junctions based on high temperature superconductors (HTS),
- classical SNS devices with a normal metal as the weak link material,
- double-barrier SNIS/INS structures.

We will briefly review the current status of all these types of junctions with emphasis on double-barrier structures. It will be shown that double-barrier structures combine advantages of weak links and tunnel junctions [8–10] and are the most promising elements for large-scale integration circuits [11–26].

Additionally, we will review the current status of the theoretical understanding of transport processes in double-barrier structures. The results of calculations will be compared with the existing experimental data.

## 2. HTS Josephson junctions

RSFQ circuits based on high- $T_C$  technology [27–39] are still quite simple since a reliable fabrication process has not been established yet to be able to produce as complex devices as in low-temperature superconductors (LTS) technology. Efforts were concentrated on the development of a technology for fabricating HTS SNS devices [40–46] and ramp type junctions with semiconductor oxides interlayers [47–59]. Unfortunately, until now the results are far from a reproducible and reliable large-scale integrated circuit technology.

### 2.1. HTS SNS junctions

The analysis of experimental data from HTS SNS step-edge Josephson junctions [60–62] has revealed that their properties are controlled by a system of highly conductive areas located at both YBCO/Au interfaces. A possible origin of these conductive areas might be related to the presence of either geometrical constrictions or resonant centers at YBCO/Au boundaries. The concentration of these pin holes at the interface perpendicular to the *ab*-planes of YBCO is about two orders of magnitude larger than the concentration at the interface perpendicular to the *c*-axis. A double constriction ScNCS model of HTS SNS devices, taking into account these features (small ‘‘c’’ and capital ‘‘C’’ denote the difference in the concentration of constrictions), has been developed and used for the interpretation of experimental data. It has been shown that the model is in good qualitative agreement with the main experimental facts: reduced  $I_C R_N$  products, linear  $I_C(T)$  curves in a broad temperature range and a similar order of magnitude of the excess and critical currents.

The random nature of the Josephson coupling of the HTS electrodes via constrictions to the noble metal interlayer makes it difficult to develop a reproducible technology for integrated circuits based on HTS SNS devices. It is for this reason that all efforts in this direction were practically stopped in 1996.

### 2.2. HTS junctions with semiconductor oxide interlayers

Edge-type junctions with an oxide ‘‘semiconductor’’ interlayer possess several advantages compared to other types of HTS Josephson junctions. Some of the semiconductor-oxide materials, e.g., PBCO, have crystal lattice parameters close to YBCO. This gives the possibility to fabricate more homogeneous interfaces compared to SNS structures.

It was found that at a rather large PBCO interlayer thickness  $d$  of 10–20 nm the normal junction resistance  $R_N$  typically exhibits a semiconductor-like temperature dependence [49–54]. That means that certain bulk properties of the semiconductor layer, rather than the boundary resistance, are dominating the junction characteristics. Moreover, it has been shown that resonant tunneling via localized states in the interlayer is responsible for the transport properties of these structures. The theoretical understanding of the normal and supercurrent transport mechanisms, taking into account the concentration of localized states in the barriers, has been developed [63–70] and was used for data interpretation. In the major number of experiments at least one of the interfaces of the YBCO/PBCO/YBCO junctions is prepared ex-situ by deposition of PBCO on the edge of the bottom electrode fabricated by ion milling. The ion beam damage of the interface influences its transport properties resulting in a suppression of its transparency and the location of a weak link at the ex-situ prepared interface. For a long time, the major technological efforts were based on the belief that a technological solution for a reproducible fabrication of this ex-situ made interface [55–59] will lead to a HTS large-scale fabrication process for integrated circuits. Really, it could be sufficient for preparing reproducible junctions, if an isotropic s-wave pairing occurs in HTS superconductors. In contrast, there is continuous experimental evidence that the

behavior of high-temperature superconductors can be understood in terms of a d-wave pairing scenario, rather than in the conventional s-wave picture.

### 2.3. *New effects at interfaces of d-wave superconductors*

The superconducting state of a d-wave superconductor in the vicinity of interfaces differs essentially from that in the bulk. The physical reason for this is the following. Due to the angular dependence of the pair potential incoming and reflected quasiparticles move in different order parameter fields. As a result, for certain directions of quasiparticle trajectories there is a sign change of the pair potential upon reflection. This sign change has fundamental consequences: it leads to the appearance of robust mid-gap states at zero energy [71]. For other trajectories, the sign of the pair potential is conserved upon reflection, while its magnitude is changed. In both cases the interface is pair-breaking and the self-consistently determined magnitude of the pair potential near the interface is reduced in comparison with its bulk value. These conclusions are still valid when the dominant d-wave order parameter in the bulk has some admixture of a (subdominant) s-wave component which is allowed by the symmetry in orthorhombic superconductors like YBCO.

As a result, several types of bound states exist near the interfaces in d-wave superconductors: (a) Robust mid-gap states at zero energy, associated with the sign change of the pair potential for certain quasiparticle trajectories [71–74]. These states lead to a peak in the density of states at the interface at zero energy. The smaller the transparency of the interface, the larger the relative height of the mid-gap states in the density of states at the interface and the stronger the zero bias anomaly (ZBA) in the conductance across the interface. (b) Andreev bound states with finite energy, which occur near the interface due to suppression of the pair potential [73]. This suppression increases with the angle between the direction of one of the principal axis and the interface. Quasiparticles are localized in the region of the order of the coherence length near the interface. This effect leads to a finite bias anomaly (FBA) in the conductance across the interface and an anomalous temperature dependence of the critical current at low temperatures.

Finally, the subdominant order parameter with s symmetry can be located in regions where the dominant order parameter is reduced [74]. If the phase of the subdominant order parameter is shifted compared to the d-wave phase, spontaneous current will flow along the boundary. In this case, the ZBA can split in zero magnetic field, as has been demonstrated experimentally [75,76]. This state will also lead to nucleation of spontaneous flux at the intersection of several boundaries [77].

The concept described above is presently the subject of intensive research. It was applied to develop the theory for the highly idealized case of specular reflecting boundaries. However, the conditions of the clean limit are not fulfilled in the vicinity of the grain boundaries or other HTS interfaces, even if the material is clean in the bulk. There are at least two reasons for that. First, the quasiparticle reflection from real interfaces is diffusive, thus, providing isotropization in momentum space and suppression of the d-wave component of the order parameter. Second, the material near the interfaces is contaminated or damaged due to the fabrication process. As a result, the formation of a thin disordered layer or a layer with different crystalline order near HTS surfaces and interfaces is highly probable.

Two approaches exist to describe the influence of disorder of quasiparticle reflection at the interfaces on the superconducting state near the boundary. First, it is assumed that the interface consists of facets with random orientations of their interface perpendicular to the *ab*-plane of the HTS material [74]. According to the second approach, both sides of the ideal interface are coated by a thin layer with a short electron mean free path [73,78]. In this case, the degree of disorder (or interface roughness) is measured by the ratio of the layer thickness to the mean free path in the layer. Recent theoretical considerations have clearly shown [79a,79b] that the formation of the layer with intensive diffusive scattering in the vicinity of HTS interfaces of HTS junctions average the peculiarities coming from the anisotropic nature of the HTS superconducting state (mid-gap states, Andreev bound states, effects associated with the breaking of time reversal symmetry). HTS junctions containing this layer will be very close to *SS'IS'S* structures with a gapless *S'* superconductor responsible for the Josephson coupling. The zero gap in the density of states leads to a suppression of all non-equilibrium effects which are

typical for ordinary s-wave superconductors. As a result, the CVC of these SS'IS'S devices should be very close to the predictions of the RSJ model [81] or, in other words, very classical. The absence of the gap should also result in more regular normal junction properties due to the suppression of Andreev reflection channels. The temperature and voltage dependencies of the junction's conductance are close to the predictions of the Glazman–Matveev theory [80] for N–Sm–N tunnel structures [81].

Therefore, in the case of a specular boundary, we have to expect an increasing spread of the critical current with decreasing dimensions of HTS Josephson junctions. In contrast, in the case of a highly diffuse boundary the spread of the critical current will be reduced. In the intermediate case, even a relatively small probability for an electron to carry out a specular reflection at the interface, will lead to the formation of d-wave shunts. The effectiveness of these processes directly follows from the one order of magnitude difference between the intensity of the d-wave and induced s-wave correlation in the vicinity of the boundaries. Thus, the critical current in this case will also be the result of averaging of the superconducting properties along the interface and will carry out mesoscopic fluctuations when the dimensions of the junction are decreased. The inhomogeneity of the superconducting parameters along the interface (probability of diffusive reflection, angle  $\alpha$  between interface normal and  $a$ -principal axis of HTS) should result in spatial variations of the superconducting properties of the electrodes in the direction perpendicular to the current flow.

The discussed model is a new source of spread of the junction's parameters which does not exist in structures based on conventional s-wave superconductors. The scale of this variations increases with an increase in the probability for specular quasiparticle reflections from the interface. It is important to note that the spreads of  $I_C$ , and  $R_N$  are controlled mainly by different physical mechanisms.

Thus, to make the parameters of HTS Josephson junctions reproducible, it is necessary not only to control the transparency of the interfaces and thickness of the weak link materials, but also the geometrical variations of the interfaces in the direction perpendicular to the current flow. This can be achieved using molecular beam epitaxy techniques to guarantee the flatness and sharpness of the interfaces on an atomic scale. An alternative solution is to introduce strong disorder at the interfaces. Both methods are very far from final implementation. Therefore, more efforts are required to develop a practical integrated technology for HTS RSFQ circuits.

### 3. LTS SNS Josephson junctions

In the last few years, interest in SNS weak links has continuously grown [82–86] since they have been considered to provide the necessary critical current density for the realization of a programmable voltage standard [87,88] in submicron technology.

The most important problem in the development of the technology for SNS junctions fabrication is the problem of the weak link material. It has to fulfill at least two opposite demands. From one point of view, to provide strong Josephson coupling at reasonably large electrode spacing, it should have a relatively large decay length

$$\xi_{nc}^* = \hbar v_F / 2\pi kT_C \quad (1)$$

(clean limit) or

$$\xi_{nd}^* = (\hbar D / 2\pi kT_C)^{1/2} \quad (2)$$

(dirty limit) and hence be a metal with a relatively large Fermi velocity  $v_F$ . Here,  $T_C$  is the critical temperature of the electrodes,  $D = v_F l / 3$  is the diffusion coefficient,  $l$  is the electron mean free path, and  $k$  the Boltzmann constant. On the other hand, these normal metals have good conductivity and their combination with Nb leads to very large values of the suppression parameter  $\gamma \geq 1$

$$\gamma = \frac{\rho_S \xi_S}{\rho_N \xi_N} \quad (3)$$

where  $\rho_{S,N}$  and  $\xi_{S,N}$  are normal resistivities and coherence lengths of S- and N-materials, respectively. Physically, this parameter compares the amount of normal electrons capable of diffusing per second from N to S to the same value of correlated electrons capable to move in the opposite direction. From theoretical calculations, it follows that at  $\gamma \geq 0.1$  strong suppression of the superconductivity at the interface takes place due to diffusion of the quasiparticles from the N-side. This results in a degradation of the weak link parameter. At smaller  $\gamma \leq 0.1$  rigid boundary conditions [89] are valid at the interface in a large temperature range, provided the junctions parameters are close to their maximal values.

Two possible candidates for the weak link materials have been suggested recently and been tested experimentally. They are PdAu alloys [82,83] and titanium [84].

In Ref. [82], Nb–PdAu–Nb junctions were made, using an in-situ deposited trilayer, consisting of a 220 nm thick Nb based electrode, a 30–50 nm thick PdAu (53% Pd, 47% Au) barrier, and a 110 nm thick Nb counter electrode. Series arrays of 400 junctions with square counter electrodes ranging from 1 to 10  $\mu\text{m}$  were used to characterize the SNS junctions. All reported measurements were done at  $T = 4.2$  K. It was found that the thickness dependence of the critical current was close to

$$J_C(d) = (385 \text{ mA}/\mu\text{m}^2) \exp\{-d/6.6 \text{ nm}\} \quad (4)$$

and the resistivity of PdAu film was  $\rho_n = 417 \text{ m}\Omega \mu\text{m}$ . From Eq. (4), we immediately calculate the decay length in PdAu

$$\xi_{nd}^* \approx 6.6 \sqrt{\frac{T}{T_C}} \approx 4.4 \text{ nm} \quad (5)$$

for  $T_C = 9.2$  K. This in combination with the typical values of the Nb resistivity ( $\rho = 2 \mu\Omega \text{ cm}$ ) and decay length  $\xi_s \approx 10$  nm gives a reasonable value of the suppression parameter  $\gamma \approx 0.1$ .

A more detailed study of the SNS junctions with PdAu interlayer was done in Ref. [83]. A  $\text{Pd}_{68}\text{Au}_{32}$  alloy layer of 42 nm thickness was used as the normal interlayer. Transport parameters of the film at  $T = 4.2$  K (density of states  $N(0) = 6.9 \times 10^{22} \text{ cm}^{-3}$ , specific resistance  $\rho = 18.25 \mu\Omega \text{ cm}$ , Fermi velocity  $1.47 \times 10^6$  m/s, electron mean free path  $l = 4.2$  nm, diffusion coefficient  $D = 20.4 \text{ cm}^{-2}/\text{s}$ ) were found from Hall measurements. A substitution of these numbers into the expressions for decay length (1) and suppression parameter (3) leads to the values  $\xi = 24.3$  nm,  $\gamma \approx 0.2$  close to that obtained in Ref. [82].

With such a small  $\gamma$  the critical current is given by the expression following from rigid boundary conditions [90]

$$I_C = \frac{64\pi T}{eR_N} C_0^2(0,T) \frac{d}{\xi_n(T)} \exp\left\{-\frac{d}{\xi_n(T)}\right\},$$

$$d \gg \xi_n(T) = \xi_{nd}^* \sqrt{\frac{T}{T_C}}, \quad (6)$$

valid at  $\gamma \ll \max\{\gamma_B, 0.2\sqrt{1 - T/T_C}\}$ . Here

$$C_0^2(0,T) = \frac{\Delta_B^2(T)}{\left[\pi T + \Delta^* + \sqrt{2\Delta^*(\pi T + \Delta^*)}\right]^2}, \quad \Delta^* = \sqrt{(\pi T)^2 + \Delta_B^2(T)},$$

$\Delta_B(T)$  is the bulk value of the pair potential and the second suppression parameter at the interface is

$$\gamma_B = \frac{R_B}{\rho_n \xi_{nd}^*}, \quad (7)$$

where  $R_B$  is the specific boundary resistance.

From the fit to experimental data, using Eq. (6), it is possible to estimate the decay length. One can rewrite Eq. (6) in the form

$$\xi_{\text{nd}}^* = d \left( \sqrt{t_1} - \sqrt{t_2} \right) \ln^{-1} \left[ \frac{C_0^2(0, t_1) t_1^{3/2} I_C(t_1)}{C_0^2(0, t_2) t_2^{3/2} I_C(t_2)} \right], \quad t_{1,2} = \frac{T_{1,2}}{T_C} \quad (8)$$

The product  $\kappa = C_0^2(0, t_1) t_1^{3/2}$  has a rather weak temperature dependence ( $0.23 \lesssim \kappa \lesssim 0.19$ ) in the temperature interval  $0.2 \leq T/T_C \leq 0.6$  with the maximum value  $\approx 0.23$  achieved at  $T/T_C \approx 0.35$ . Fixing  $t_1 = 0.4$  and with the corresponding experimental value of the critical current  $I_C = 7.36 \mu\text{A}$  and changing  $t_2$  and  $I_C$  in Eq. (8) in accordance with the data we obtained  $\xi_{\text{nd}}^* \approx 6.8 \text{ nm}$ . This is four times smaller than the value followed from the measured lateral transport constants of the weak link material. This difference correlates with the experimental fact [83] that the normal resistance is several times larger than the value calculated making use of the geometry of the junction and specific resistivity estimated from the Hall measurements.

This means that certain interface properties rather than bulk normal metal properties are responsible for the real junction parameters, making the behavior of the structures close to that of the double-barrier devices. The same conclusion follows from the analysis of the data obtained in Ref. [84] for Nb–Ti–Nb SNS junctions. The parameters of Nb–Ti–Nb and Nb–Pd<sub>68</sub>Au<sub>32</sub>–Nb are summarized in Table 1.

It follows from Table 1, that to achieve a reasonable value for the critical current density it is necessary to fabricate junctions with a normal metal thickness  $d$  smaller than  $\xi_{\text{nd}}^* \lesssim 5 \text{ nm}$ . This estimate shows that the problem of controlling the interface properties is even more important than in realized structures [83,84] since the difference in lateral and vertical transport in the devices cannot be understood in terms of a simple mismatch of the Fermi velocities at the interfaces. For the mismatch  $\lesssim 0.5$  and typical value of the Fermi momentum  $p_F \approx 10^{-24} \text{ kg/s}$  the specific boundary resistance is very low,  $R_B \approx 10^{-13} \Omega \text{ cm}^2$ , and the contribution from the boundaries to the total  $R_N$  is then smaller than 0.1%. The real reason for the large interface resistance can be associated with deterioration of the interface between N and S materials during the fabrication process originating from a region of mixed composition. In the case of Nb/Al/Nb sandwiches for a Al thickness lower than 15 nm no clear Al layer existed, because of diffusion of about 7–10 nm between the Nb top film and Al [85,86]. The diffusion of 3–5 nm between lower Nb and Al has also been found in Ref. [86]. Moreover, the deposition of a thin Al ( $\approx 10 \text{ nm}$ ) film on top of thick Nb is accompanied by the formation of an interface with a finite transparency [91,92], which corresponds to a suppression parameter  $\gamma_B \approx 1$ . The intermixing of the materials at the boundaries results in a strong reduction of the electron mean free path in the formed boundary layer. This, in turn, provides strong backscattering of electrons and, hence, noticeable boundary resistance. The thickness of the boundary layer depends on the morphology of the interfaces. For Nb thin films with a thickness of  $d_s \approx 150\text{--}200 \text{ nm}$  the surface roughness (in the absence of surface planarization of the base electrode [91,93,94]) is of the order of 3–5 nm. This value is comparable with the decay lengths in the weak link normal metals.

Thus, to fabricate reproducible SNS weak links for large-scale integrated circuits, it is necessary to develop a technology that is able to control the mentioned interface resistance and to guarantee the flatness of the interfaces at the scale smaller than at least 1 nm, as well as the absence of interdiffusion of N and S materials on the same scale.

To our mind, at the present level of technology, these problems can be solved by the fabrication of artificial boundaries making use of stable normal metal oxides to define the interfaces in SNS devices. Right now, these

Table 1  
Parameters of Nb–Ti–Nb<sup>84</sup> and Nb–Pd<sub>68</sub>Au<sub>32</sub>–Nb<sup>83</sup> SNS weak links ( $T = 4.2 \text{ K}$ )

Reference	$S$ ( $\mu\text{m}^2$ )	$R_N$ (m $\Omega$ )	$\rho_{\text{lat}}$ ( $\mu\Omega \text{ cm}$ )	$\rho_{\text{ver}}$ ( $\mu\Omega \text{ cm}$ )	$\xi_{\text{nd}}^*$ (nm)	$d$ (nm)	$\gamma$	$I_C$ (mA)	$J_C$ (kA/cm <sup>2</sup> )	$I_C R_N$ ( $\mu\text{V}$ )
[83]	6.25	19	18	180	6.8	42	0.2	6	96	110
[84]	16	1.7	50–200	80	4.8	35	0.06	4.7	29	8

double-barrier SINIS structures demonstrate high reproducibility and ability to be used in large-scale integrated circuits [12,13,17].

#### 4. SS'IS'IS'S double-barrier Josephson junctions

Double-barrier SS'IS'IS'S structures are unique devices with properties that make use of the main advantages from weak links and tunnel-type devices [8].

(1) They are intrinsically shunted. This means that all nonlinear properties in SS'IS'IS'S junctions are located in the S' interlayer making the CVC non-hysteretic and close to RSJ or “classical weak link” type.

(2) The normal resistance of the junction is mainly controlled by the barriers rather than by the transport properties of the interlayer materials. This makes the problem of impedance matching between the junctions and transmission lines easier to solve. The spread of  $R_N$  is given only by the lateral homogeneity of the two  $\text{AlO}_x$  barriers, which are prepared by thermal oxidation.

(3) The increase of the barrier transparencies up to a level accompanied by the formation of pin holes will not lead to large spread of the parameters due to averaging of the pin hole contributions at two interfaces.

(4) The oxide layers clearly define the interface between S' and S materials, making the problem of interdiffusion between S' and S materials as in SNS devices of less importance.

(5) The SS'IS'IS'S junctions are successfully used for fabrication of microcircuits for voltage standards (more than 8000 junctions) and simple RSFQ circuits with an on-chip spread of junction parameters smaller than 10%.

Summarizing the above analysis, we can conclude that double-barrier structures are the most attractive devices for the fabrication of large-scale superconducting circuits. In the next sections, we will focus on the description of the transport processes in these structures and on the current experimental and technological status.

##### 4.1. Stationary properties of SIS'IS junctions in the dirty limit

If the conditions of the dirty limit (electron mean free path  $l \ll d, \xi_{\text{nd}}^*$ ) are fulfilled in the S' interlayer, then the stationary Josephson effect in the structure can be analyzed in the framework of the Usadel equations [8–10]. For narrow junctions with a width  $W$  in the direction perpendicular to the current flow smaller than the Josephson penetration depth  $\lambda_J$  and for transparencies of interfaces small enough to provide the inequality  $\gamma \ll \gamma_B$  between the suppression parameters (3), (7) at both interfaces the  $I(\varphi)$  relationship in the limit  $d \ll \xi_{\text{nd}}^*$  has the form

$$\frac{IR_N}{2\pi T_C} = \frac{T}{\gamma_{\text{eff}} T_C} \left\{ \sum_{\omega \geq 0} \frac{f^2}{\omega^2 + f^2} \frac{\pi T_C}{\sqrt{\omega^2(1+q)^2 + [qf\eta(\varphi) + \Delta]^2}} \right\} \sin(\varphi) + \frac{T}{T_C} \left\{ \sum_{\omega \geq 0} \frac{f}{\sqrt{\omega^2 + f^2}} \frac{\Delta}{\sqrt{\omega^2(1+q)^2 + [qf\eta(\varphi) + \Delta]^2}} \right\} \frac{\sin(\varphi)}{\eta(\varphi)}, \quad (9)$$

$$q = \frac{g}{\gamma_{\text{eff}} \Omega}, \quad \eta(\varphi) = \sqrt{\cos^2\left(\frac{\varphi}{2}\right) + \gamma_-^2 \sin^2\left(\frac{\varphi}{2}\right)},$$

$$\gamma_{\text{eff}} = \frac{\gamma_{B2} \gamma_{B1}}{\gamma_{B2} + \gamma_{B1}} \frac{d}{\xi_{\text{nd}}^*}, \quad \gamma_- = \frac{\gamma_{B1} - \gamma_{B2}}{\gamma_{B2} + \gamma_{B1}}, \quad \Omega = \frac{\omega}{\pi T_C}.$$

Here,  $f$  and  $g$  are the absolute values of the Green's functions in the superconducting banks,  $\omega = \pi T(2n + 1)$  are the Matsubara frequencies,  $\Delta$  is the modulus of the order parameter of the interlayer which should satisfy the self-consistency equation

$$\Delta \left\{ \ln \frac{T}{T_C^*} + 2\pi T \sum_{\omega \geq 0} \left[ \frac{1}{\omega} - \frac{1}{\sqrt{\omega^2(1+q)^2 + [qf\eta(\varphi) + \Delta]^2}} \right] \right\} = 2\pi T \sum_{\omega \geq 0} \left[ \frac{qf\eta(\varphi)}{\sqrt{\omega^2(1+q)^2 + [qf\eta(\varphi) + \Delta]^2}} \right]. \quad (10)$$

Here,  $T_C^*$  is the critical temperature of the interlayer metal. If the superconducting banks are spatially homogeneous,  $f = \Delta_B$  and  $g = \omega/\sqrt{\Delta_B^2 + \omega^2}$ , where  $\Delta_B$  is the bulk pair potential in S the material.

From Eqs. (9) and (10), it follows that there are two mechanisms for Josephson coupling in the SIS'IS structure. The first term in Eq. (9) describes the direct interaction between the superconducting banks, while the second shows that there is also a contribution to the current due to sequential tunneling in two SIS' junctions connected in series. The interplay between these two channels depends on the value of the suppression parameters, temperature interval and the ratio of the critical temperatures of S and S' metals.

#### 4.1.1. Limit of high temperatures

If the temperature is large enough to guarantee the inequality

$$\pi T \gg \frac{\gamma_{\text{eff}}}{1 + \gamma_{\text{eff}}} \Delta + \frac{1}{1 + \gamma_{\text{eff}}} f, \quad (11)$$

then it follows from Eqs. (9) and (10) that in this temperature interval the modulus of the interlayer order parameter  $\Delta \propto \eta(\varphi)$  and, hence, the  $I(\varphi)$  relationship has a sinusoidal form,  $I(\varphi) \propto \sin(\varphi)$ . If we suppose further that  $T$  is close to the critical temperature of the superconducting electrodes and  $f = \Delta_B$ , then the self-consistency Eq. (10) has the analytical solution

$$\Delta = \Delta_B \eta(\varphi) \frac{p(\gamma_{\text{eff}})}{p(\gamma_{\text{eff}}) + \ln(T_C/T_C^*)}, \quad p(\gamma_{\text{eff}}) = \psi\left(\frac{1}{2} + \frac{1}{2\gamma_{\text{eff}}}\right) - \psi\left(\frac{1}{2}\right), \quad (12)$$

$$\frac{IR_N}{2\pi T_C} = \frac{\Delta_B^2 \sin(\varphi)}{(\pi T_C)^2} \left\{ \sum_{n \geq 0} \frac{1}{(2n+1 + \gamma_{\text{eff}}(2n+1)^2)} \left[ \frac{\gamma_{\text{eff}} p(\gamma_{\text{eff}})}{p(\gamma_{\text{eff}}) + \ln(T_C/T_C^*)} + \frac{1}{(2n+1)} \right] \right\}. \quad (13)$$

In the limit of small ( $\gamma_{\text{eff}} \ll 1$ ) and large ( $\gamma_{\text{eff}} \gg 1$ ) values of the suppression parameter the  $I(\varphi)$  relationship has the forms, respectively

$$\frac{IR_N}{2\pi T_C} = \frac{\Delta_B^2}{(\pi T_C)^2} \left\{ \frac{\pi^2}{8} + \frac{\gamma_{\text{eff}}}{2} \frac{\ln^2(1/2\gamma_{\text{eff}})}{\ln(T_C/2\gamma_{\text{eff}}T_C^*)} \right\} \sin(\varphi), \quad (14)$$

$$\frac{IR_N}{2\pi T_C} = \frac{\Delta_B^2}{\gamma_{\text{eff}}(\pi T_C)^2} \left\{ \frac{\pi^2}{8} \frac{\gamma_{\text{eff}} \pi^2/4}{\pi^2/4 + \gamma_{\text{eff}} \ln(T_C/T_C^*)} + \sum_{n \geq 0} \frac{1}{(2n+1)^3} \right\} \sin(\varphi). \quad (15)$$

In the zero approximation of the parameter  $\gamma_{\text{eff}}$ , expression (14) coincides with the well-known results of the Aslamazov–Larkin weak link theory [96] thus demonstrating that in this limit the properties of the SIS'IS structure are practically independent of the material constants of the interlayer.

In contrast to that, in the practically interesting case of large  $\gamma_{\text{eff}}$ , it follows from Eq. (15) that the characteristic voltage  $V_C = I_C R_N$  depends on the product  $\gamma_{\text{eff}} \ln(T_C/T_C^*)$  and the strength of the suppression parameter  $\gamma_{\text{eff}}$  starts to be effectively screened at  $T_C^* \gtrsim (1/30)T_C$ . Hence, we must expect the noticeable enhancement of the  $I_C R_N$  product with an increase of the interlayer critical temperature.

#### 4.1.2. Limit of low temperatures

If  $T \ll T_C^*$  and  $T_C \ll \gamma_{\text{eff}} T_C^*$  then  $qf\eta(\varphi) \ll \Delta$  and in the first approximation of parameters

$$\mu = \frac{qf\eta(\varphi)}{\Delta} \approx \frac{T_C}{\gamma_{\text{eff}} T_C^*} \ll 1, \text{ and } q \ll 1$$

the solution of Eq. (10) has the form

$$\Delta = \Delta(T) + S_1/S_2, \quad (16)$$

$$S_1 = 2\pi T \sum_{\omega \geq 0} \left[ \frac{\omega^2(\mu - q)}{(\omega^2 + \Delta^2(T))^{3/2}} \right], \quad S_2 = 2\pi T \sum_{\omega \geq 0} \left[ \frac{1}{(\omega^2 + \Delta^2(T))^{3/2}} \right],$$

where  $\Delta(T)$  is the bulk pair potential of the interlayer material.

Substitution of Eq. (16) into the expression for the supercurrent (9) results in the  $I(\varphi)$  relationship that exactly coincides with the expression for structures consisting of two SIS' junctions in series

$$\frac{IR_N}{2\pi T_C} = \frac{T}{T_C} \left\{ \sum_{\omega \geq 0} \frac{f}{\sqrt{\omega^2 + f^2}} \frac{\Delta}{\sqrt{\omega^2 + \Delta^2(T)}} \right\} \frac{\sin(\varphi)}{\eta(\varphi)}. \quad (17)$$

The critical current is achieved at

$$\cos(\varphi) = \min \left\{ \frac{\gamma_{B1}}{\gamma_{B2}}, \frac{\gamma_{B2}}{\gamma_{B1}} \right\} \quad (18)$$

and is given by

$$\frac{IR_N}{2\pi T_C} = \frac{T}{T_C} \left\{ \sum_{\omega \geq 0} \frac{f}{\sqrt{\omega^2 + f^2}} \frac{\Delta}{\sqrt{\omega^2 + \Delta^2(T)}} \right\} \frac{\gamma_{B1} + \gamma_{B2}}{\max\{\gamma_{B1}, \gamma_{B2}\}}. \quad (19)$$

Thus, in this limit, the channel of sequential tunneling is dominating over the channel of direct coupling and the SIS'IS structure behaves like two tunnel SIS' junctions in series.

#### 4.1.3. Limit of small suppression parameter

For smaller  $\gamma_{\text{eff}}$

$$\gamma, \frac{d_2}{\xi_{\text{nd}}^{*2}} \ll \gamma_{\text{eff}} \ll 1 \quad (20)$$

in a first approximation of  $\gamma_{\text{eff}}$  the supercurrent does not depend on the superconducting properties of the interlayer material and Eq. (9) is reduced to

$$\frac{IR_N}{2\pi T_C} = \frac{T}{T_C} \sum_{\omega \geq 0} \frac{f^2 \sin(\varphi)}{\sqrt{\omega^2 + f^2} \sqrt{\omega^2 + [f\eta(\varphi)]^2}}. \quad (21)$$

This expression is only slightly different from the one for SIS tunnel junctions and transforms to it if we take  $\eta(\varphi) = 1$ . As soon as the coefficient  $\eta(\varphi) \leq 1$  at any  $\varphi$  we immediately obtain that in this particular limit (20) the  $I_C R_N$  product of SIS'IS junctions is larger than the characteristic voltage of SIS structures in the whole temperature interval. In particular, at  $T = 0$  after integration over  $\omega$  in Eq. (20) we arrived at

$$\frac{IR_N}{2\pi T_C} = \frac{\Delta(0)}{2\pi T_C} K\left(\sqrt{1 - \gamma_-^2} \sin\left(\frac{\varphi}{2}\right)\right) \sin\left(\frac{\varphi}{2}\right) \quad (22)$$

where  $K(z)$  is the elliptic integral of the first kind. At  $\gamma_- = 0$ , critical current in Eq. (22) is achieved at  $\varphi = 1.86$  with a  $I_C R_N$  product 22% larger than in SIS junctions and 8% smaller than predicted by the KO-1 theory [97] for dirty SNS weak links.

The physical reason of this result is the following. In the regime (20), the real part of the anomalous Green's function  $f$  is constant across the structure due to the proximity effect between the electrodes and the interlayer. This means that despite the existence of the two barriers in the junction, strong correlation between them makes the structure practically a single-barrier device. In Section 4.2, this result will also be proved exactly in the clean limit.

#### 4.1.4. Limit of large suppression parameter

In the limit of a large value of the suppression parameter  $\gamma_{\text{eff}}$ , there are three characteristic temperature intervals in the  $I_C(T)$  dependence.

At temperatures larger than the critical temperature of the interlayer material

$$\frac{T}{T_C^*} \geq 1 + \left[ \frac{\sqrt{T_C(T_C - T_C^*)}}{\gamma_{\text{eff}} T_C^*} \right]^{2/3} \quad (23)$$

the current–phase relationship has the  $\sin(\varphi)$  form

$$\frac{IR_N}{2\pi T_C} = \frac{T \sin(\varphi)}{\gamma_{\text{eff}} T_C} \left\{ \sum_{\omega \geq 0} \frac{f^2 \pi T_C}{\omega(\omega^2 + f^2)} + \frac{2\pi^2 T T_C}{\ln(T/T_C^*)} \left\{ \sum_{\omega \geq 0} \frac{f}{\omega \sqrt{\omega^2 + f^2}} \right\}^2 \right\} \quad (24)$$

and the  $I_C R_N$  product is proportional to  $\gamma_{\text{eff}}^{-1}$ .

In the rather small temperature interval in the vicinity of  $T_C^*$

$$\left| \frac{T}{T_C^*} - 1 \right| \lesssim \left[ \frac{\sqrt{T_C(T_C - T_C^*)}}{\gamma_{\text{eff}} T_C^*} \right]^{2/3} \quad (25)$$

the term proportional to  $\ln(T/T_C^*)$  in the left hand side of the self-consistency Eq. (10) can be neglected resulting in

$$\frac{IR_N}{2\pi T_C} = \frac{1}{\gamma_{\text{eff}}^{1/3}} \frac{T}{T_C} \left\{ \sum_{\omega \geq 0} \frac{f}{\omega \sqrt{\omega^2 + f^2}} \right\} \left[ \frac{S_3}{S_4} \right]^{1/3} \frac{\sin(\varphi)}{(\eta(\varphi))^{2/3}}, \quad (26)$$

where

$$S_3 = 2\pi T \sum_{\omega \geq 0} \frac{\pi T_C f}{\omega \sqrt{\omega^2 + f^2}}, \quad S_4 = 2\pi T \sum_{\omega \geq 0} \frac{1}{\omega^3}. \quad (27)$$

Thus, in the vicinity of  $T_C^*$ , we must expect an essential increase of the  $I_C R_N$  product caused by the transformation from an  $I_C R_N \propto \gamma_{\text{eff}}^{-1}$  law to an  $I_C R_N \propto \gamma_{\text{eff}}^{-1/3}$  one. Unfortunately, this amplification is accompanied by the modification of the  $I(\varphi)$  relationship. Still, a temperature interval above  $T_C^*$  exists in which the deviation from  $I(\varphi) \propto \sin(\varphi)$  is small, while  $I_C R_N$  product has values larger than would follow from Eq. (24).

Finally, at temperatures

$$\frac{T}{T_C^*} \leq 1 - \left[ \frac{\sqrt{T_C(T_C - T_C^*)}}{\gamma_{\text{eff}} T_C^*} \right]^{2/3} \quad (28)$$

the cross-over to the low-temperature regime described by Eq. (19) takes place.

#### 4.1.5. Critical current of the individual interface

In the temperature interval  $T \leq T_C^*$ , the interlayer material is in the superconducting state and it is experimentally possible to apply a supercurrent across one of the interfaces of the double-barrier structure. If we suppose that the supercurrent flows through interface number one, than from the condition  $I_2 = 0$  it is easy to show that

$$\chi = \frac{\varphi}{2} + \arcsin \left( \frac{S_5}{S_6} \sin(\varphi) \right), \quad (29)$$

where

$$S_5 = \sum_{\omega \geq 0} \frac{Gf^2}{\gamma_{B2} \gamma_{B1} G\beta^2(d/\xi_{\text{nd}}^*) + g(\gamma_{B2} + \gamma_{B1})},$$

$$S_6 = \sum_{\omega \geq 0} \frac{\gamma_{B1} G^2 f \Delta(d/\xi_{\text{nd}}^*)}{\gamma_{B2} \gamma_{B1} G\beta^2(d/\xi_{\text{nd}}^*) + g(\gamma_{B2} + \gamma_{B1})}$$

and

$$I_1 = \frac{\sigma 2\pi T}{\xi_{\text{nd}}^*} \left\{ \sum_{\omega \geq 0} \frac{Gf^2 \omega \sin(\varphi) + G^2 f \gamma_{B2} \Delta(d/\xi_{\text{nd}}^*) \sin(\varphi + \arcsin\{(S_5/S_6) \sin(\varphi)\})}{\gamma_{B2} \gamma_{B1} G\beta^2(d/\xi_{\text{nd}}^*) + g(\gamma_{B2} + \gamma_{B1})} \right\}. \quad (30)$$

Here,  $\beta^2 = \omega/\pi T_C$ ,  $G$  is the normal Green's function of the interlayer material. It is seen from Eq. (30) that in the experimentally interesting case  $\gamma_{B1}(d/\xi_{\text{nd}}^*) \gg 1$  there is a  $\sin(2\varphi)$  correction to the  $I \propto \sin(\varphi)$  law in Eq. (30).

#### 4.1.6. Arbitrary values of the parameters

At arbitrary values of the junction parameters, the self-consistency Eq. (10) was solved numerically. The temperature dependence of the  $V_C = I_C R_N$  product calculated for  $T/T_C^* = 1.25$  and different values of the suppression parameter  $\gamma_{\text{eff}}$  is shown in Fig. 1.

The dashed line in Fig. 1 illustrates the  $V_C(T)$  dependence as calculated for a single-barrier SIS junction. The curve for SISIS (two SIS in series) would be twice as large as in the SIS case, since the normal junction

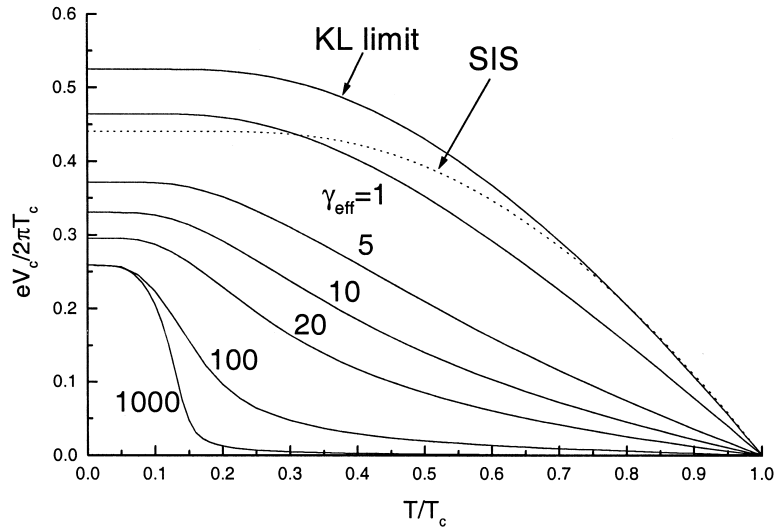


Fig. 1. Temperature dependence of the characteristic voltage  $V_C = I_C R_N$  of SIS'IS double-barrier devices, calculated in the framework of the Usadel equations for  $T_C^* = 1.25$  and different values of the suppression parameter  $\gamma_{\text{eff}}$ .

resistance of SISIS structure has a twice larger  $R_N$  as the SIS contact. It is clearly seen from Fig. 1, that at  $\gamma_{\text{eff}} \lesssim 1$  there is a large temperature interval in which the  $I_C R_N$  product of double-barrier structure is even larger compared to this value in classical SIS tunnel structures. Increase of the suppression parameter leads to a decrease of  $I_C R_N$  product. It is important to note that at  $T/T_C \approx 0.5$  and  $\gamma_{\text{eff}} \approx 20$ , as well as at  $T/T_C \approx 0.2$  and  $\gamma_{\text{eff}} \approx 100$  the ratio  $V_{C(\text{SIS})}/V_{C(\text{SIS'IS})}$  is only of the order of 4, while the  $I(\varphi)$  relationship still has the classical  $\sin(\varphi)$  form. The closer the critical temperature of the interlayer to the helium temperature, the larger the interval of parameters in double-barrier structures with reasonable values of the characteristic voltage  $V_C$  and a behavior typical to the classical Josephson structures.

Fig. 2 gives the dependence of the  $I_C R_N$  product on the ratio of critical temperatures  $T_C^*/T_C$  calculated for different values of the suppression parameter  $\gamma_{\text{eff}}$  and at the helium temperature  $T/T_C = 0.46$  in the case of the S being Nb. Here, it is seen again that for small  $\gamma_{\text{eff}}$  the critical voltage is independent of the critical temperature ratio, while for large  $\gamma_{\text{eff}}$  this dependence is strong. For equal critical temperatures of S and S' and for large  $\gamma_{\text{eff}}$  the total structure behaves at this temperature as two equal tunnel junctions in series.

The performed theoretical analysis is essentially based on the assumption that the condition of the dirty limit is fulfilled in the interlayer material. On the other hand, recent systematic study of transport parameters of thin Al films in Nb/Al/AIO<sub>x</sub>/Al/Nb tunnel structures [92] has shown that they are mainly controlled by electron scattering at the interfaces, resulting in the following phenomenological relation between the electron mean free path  $l_{\text{Al}}$  and the thickness  $d_{\text{Al}}$  of the film

$$l_{\text{Al}} \approx 0.84 d_{\text{Al}} - 0.00276 d_{\text{Al}}^2. \quad (31)$$

It demonstrates that the assumption of the dirty limit is difficult to justify and motivates us to consider the properties of double-barrier structures in the clean limit as well.

#### 4.2. Stationary properties of SIS'IS junctions in the clean limit

Here, we present the results of a theoretical study of the universal features of a supercurrent in a three-dimensional SIS'IS junction in the clean limit. Previous theoretical work on ballistic SINIS structures was

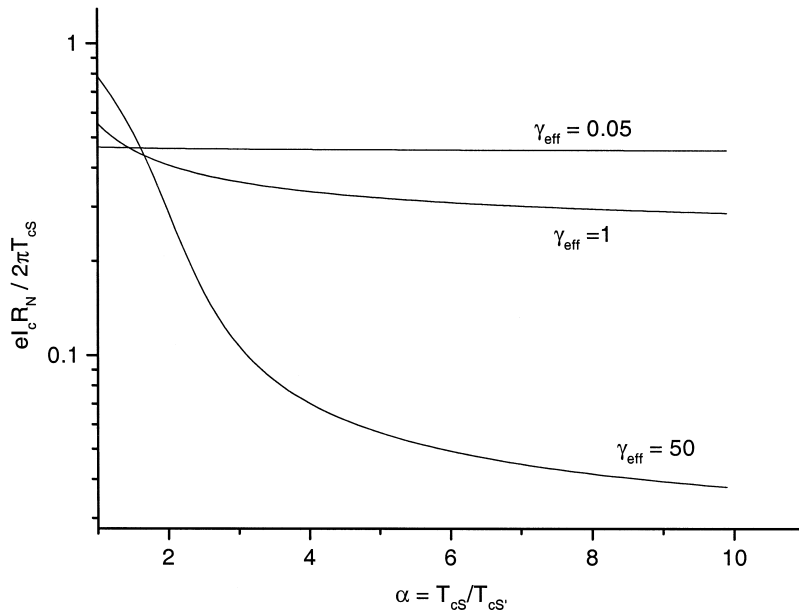


Fig. 2.  $I_c R_N$  product of SIS'IS double-barrier devices as a function of the ratio of the interlayer critical temperature ( $T_C^*$ ) to the critical temperature of the electrodes ( $T_C$ ) calculated in the framework of the Usadel equations for different suppression parameters,  $\gamma_{\text{eff}}$ , at the helium temperature ( $T/T_C = 0.46$ ).

concentrated on studying resonant supercurrents in low-dimensional structures [99–102]. We demonstrate that at a small suppression parameter the coherent regime takes place when the supercurrent is proportional to the single barrier transparency  $D$ , while for a large suppression parameter it becomes of the order of  $D^2$ , as expected for two uncorrelated sequential tunneling processes. We study quantitatively the cross-over between these two regimes and the relation to the dirty limit results obtained above. It is important, that in the coherent regime both models provide identical results, while for large suppression parameters simple scaling is found. Furthermore, we show that the coherent supercurrent can be derived from the distribution of transmission eigenvalues  $\rho(D) = (G_N/\pi G_0)D^{-3/2}(1-D)^{-1/2}$  known for a two-barrier  $\text{NI}_1\text{NI}_2\text{N}$  junction [103], where  $G_0 = e^2/2\pi\hbar$  and  $G_N$  is the total junction conductance.

We consider a ballistic  $\text{SI}_1\text{S}'\text{I}_2\text{S}$  contact with  $T_C^* < T_C$  and mean free path  $l'_s \gg d$ , where  $d$  is the interlayer thickness and  $I_{1,2}$  are parallel atomically sharp interfaces with arbitrary transmission coefficients. In the temperature Green's function method, the supercurrent density  $J_s$  is expressed through the Fourier transform of the Green's function  $G(\mathbf{r}, \mathbf{r}')$  over the coordinates along the junction plane [104]

$$I_s = \frac{i\hbar e}{m} \int \frac{d^2 k_{\parallel}}{(2\pi)^2} T \sum_{\omega_n > 0} \lim_{x' \rightarrow x} \left( \frac{\partial}{\partial x'} - \frac{\partial}{\partial x} \right) G(x, x'), \quad (32)$$

where  $x, x'$  are the coordinates across the junction,  $k_{\parallel}$  is the wave-vector component in the junction plane and  $\omega = (2n+1)\pi T$  are Matsubara frequencies. The normal and the anomalous Green's functions  $G(x, x')$ ,  $F^+(x, x')$  obey the Gor'kov equations [104]

$$\begin{pmatrix} i\omega + H & \Delta(x) \\ \Delta^*(x) & i\omega - H \end{pmatrix} \begin{pmatrix} G \\ F^+ \end{pmatrix} = \begin{pmatrix} \delta(x-x') \\ 0 \end{pmatrix} \quad (33)$$

where  $H = (\hbar^2/2m)(\partial^2/\partial x^2) + E_{\perp} - V(x)$ ,  $\Delta(x)$  is the pair potential,  $E_{\perp} = \mu - \hbar^2 k_{\parallel}^2/2m$  is the electron kinetic energy across the junction,  $V(x) = W_1 \delta(x) + W_2 \delta(x-d)$  is the interface potential,  $W_{1,2}$  being the barrier strengths.

Solving the Gor'kov equations in S and S' regions and matching the solutions at the interfaces we arrive at the expression for the supercurrent  $J_S$  valid for arbitrary  $d$  and  $W_{1,2}$ , which is written down below for the case of a thin interlayer  $d < \xi_{nc}^*$  and symmetric low-transparent barriers  $W_{1,2} = W$ ,  $(W/\hbar v_F) \gg 1$

$$I_S = \frac{e}{\hbar} \int \frac{d^2 k_{\parallel}}{(2\pi)^2} T \sum_{\omega \geq 0} \frac{\Delta_B^2 \sin \varphi + \Delta_B \Delta \sqrt{E_1/E_2} d \tilde{W}^2 / (x^3 \xi_{nc}^*) \sin \varphi / 2}{2 \tilde{W}^4 E_1^2 (\cosh d / (\xi_{nc}^* x) - \cos 2k_F dx) + E_3^2}. \quad (34)$$

Here,  $\varphi$  is the phase difference across the junction,  $\Delta_B$ ,  $\Delta$  are the pair potentials in S and S',  $E_1 = \sqrt{\omega^2 + \Delta_B^2}$ ,  $E_2 = \sqrt{\omega^2 + \Delta^2}$ ,  $E_3 = \sqrt{\omega^2 + \Delta_B^2 \cos \varphi / 2}$ ,  $\tilde{W} = W/\hbar v_F$ ,  $\xi_{nc}^* = \hbar v_F / 2\pi T_C$  is the clean limit coherence length in S' and  $x = \cos \theta$ , where  $\theta$  is the angle with the interface normal. The result (34) is valid for any shape of an atomically sharp interface barrier potential. Eq. (34) can be also applied to the resonant supercurrent in low-dimensional contacts by changing the phase space in integration over  $k_{\parallel}$ . In relevant limits, the results of [99–102] can be reproduced. Here, we concentrate on the 3D case.

To compare the results with findings of the model for the dirty limit, we define the suppression parameter

$$\gamma_{\text{eff}} = 4 \left( \tilde{W}_1^2 + \tilde{W}_2^2 \right) \frac{d}{\xi_{nc}^*} = \frac{1}{\langle xD(x) \rangle} \frac{d}{\xi_{nc}^*} \equiv \frac{d}{\langle xD(x) \rangle} \frac{2\pi T_C}{\hbar v_F}. \quad (35)$$

This definition coincides with that for the dirty limit model. Here, the angle-averaged junction transparency is given by  $D \equiv \langle xD(x) \rangle = D_1 D_2 / (D_1 + D_2) = 1/4(\tilde{W}_1^2 + \tilde{W}_2^2)$ , where single-barrier transparencies are  $D_{1,2} = \langle xD_{1,2}(x) \rangle = \tilde{W}_{1,2}^2/4$ . In the dirty limit, the suppression parameter is defined by Eq. (7) and can be written in the form  $\gamma_B = 2\pi T_C d / \hbar v_F \langle xD(x) \rangle$  which coincides with Eq. (35).

As follows from Eq. (34), the relation between the direct and sequential coupling depends on the value of  $\gamma_{\text{eff}}$ . The coherent regime (direct coupling dominates) takes place in the limit of small values of the suppression parameter  $\gamma_{\text{eff}} \ll 1$ . The supercurrent is then given by

$$I_S = \frac{e}{\hbar} \int \frac{d^2 k_{\parallel}}{(2\pi)^2} T \sum_{\omega} \frac{\Delta_B^2 \sin \varphi}{E_1^2 D^{-1} - \Delta_B^2 \sin^2 \varphi / 2}, \quad (36)$$

where the total junction transparency  $D$  in a normal state has the resonant structure:  $D^{-1} = 1 + (2\tilde{W} \cos k_F dx + 2\tilde{W}^2 \sin k_F dx)^2$ . Integration over the directions of  $k_{\parallel}$  (over the resonances) yields the supercurrent

$$\frac{I_S R_N}{2\pi T_C} = \frac{T}{T_C} \sum_{\omega} \frac{\Delta_B^2 \sin \varphi}{\sqrt{\omega^2 + \Delta_B^2} \sqrt{\omega^2 + \Delta_B^2 \cos^2 \varphi / 2}}, \quad (37)$$

which does not depend on the properties of the interlayer and coincides exactly with the dirty-limit expression (21) under the substitution  $f = \Delta_B$ . Here,  $R_N^{-1} = e^2 k_F^2 \langle xD(x) \rangle / 4\pi^2 \hbar$  is the specific contact resistance. In the coherent regime, the dominant contribution to the supercurrent comes from the transmission resonances and as a result the supercurrent is of the first order in  $\langle xD(x) \rangle$  and  $I_C R_N$  product in this case is even larger than that in the SIS tunnel junction. One can also see that in this regime the electron mean free path does not play a role as does neither one of the material parameters of the interlayer.

In the limit of large values of the suppression parameter  $\gamma_{\text{eff}} \gg 1$ , the coherent regime breaks down for  $d/\xi_{nc}^* \tilde{W}^2 \geq 1$  due to dephasing of the transmission resonances. As follows from Eq. (34) for  $T \gg T_C^*$ , the

supercurrent becomes of the order of  $\langle xD(x) \rangle^2$  as expected for the incoherent tunneling in a double-barrier contact. In this regime

$$\frac{I_S R_N}{2\pi T_C} = \frac{16}{7\gamma_{\text{eff}}} \frac{T}{T_C} \sum_{\omega} \frac{\pi T_C \Delta_B^2 \sin \varphi}{\omega(\omega^2 + \Delta_B^2)}. \quad (38)$$

It is seen from comparison of Eqs. (38) and (24) that in the limit of large values of the suppression parameter the ratio of the supercurrents in the clean limit and the dirty limit is temperature-independent at  $T \gg T_C^*$  and is given by a factor of 16/7, which reflects different ways of angle averaging in the S' interlayer in the two limits. That means, that the dirty limit model is justified also in the regime  $\gamma_{\text{eff}} \gg 1$  as long as one takes this correction factor into account. For arbitrary parameter values, the relation between the two models can be calculated numerically. The cross-over is shown in Fig. 3, where  $I_C R_N$  vs.  $\gamma_{\text{eff}}$  is plotted for both models at different temperatures. The figure clearly shows that the curves coincide for  $\gamma_{\text{eff}} < 0.1$  and scale with the factor 16/7 for  $\gamma_{\text{eff}} > 10$ .

Note that the supercurrent in the coherent regime for the energies  $|\Delta_B| \cos \varphi/2 < \varepsilon < |\Delta_B|$  has the spectral density  $\text{Im } I_S(\varepsilon) = \Delta_B^2 \sin \varphi / \sqrt{\Delta_B^2 - \varepsilon^2} \sqrt{\varepsilon^2 - \Delta_B^2 \cos^2 \varphi/2}$ , while  $\text{Im } J_S(\varepsilon) = 0$  for  $\varepsilon < |\Delta_B| \cos \varphi/2$  and  $\varepsilon > |\Delta_B|$ , i.e., the Andreev bound states in the energy range  $|\Delta_B| \cos \varphi/2 < \varepsilon < |\Delta_B|$  contribute to the supercurrent. Interestingly, this result can be derived from the distribution of transmission eigenvalues for the two-barrier NININ contacts

$$\rho(D) = (G_N/\pi G_0) D^{-3/2} (1-D)^{-1/2}, \quad (39)$$

where  $G_0 = e^2/2\pi\hbar$ . This is proven by the direct calculation of the integral  $\int_0^1 I_C(D) \rho(D) dD$ , where  $I_C(D)$  is a supercurrent per single ballistic channel,  $I_C(D) = (e/2\hbar) |\Delta_B|^2 D \sin \varphi \tanh(E_B/2T)/E_B$  and  $E_B = \Delta\sqrt{1-D \sin^2 \varphi/2}$  is the bound state energy. It yields exactly the coherent supercurrent of Eq. (37).

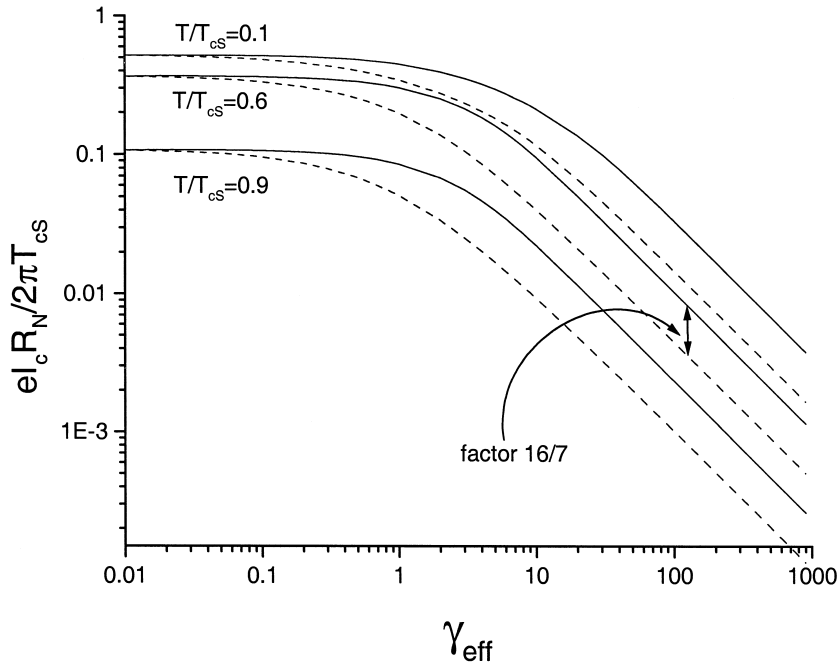


Fig. 3. Relation between the normalized critical voltage and the suppression parameter for a double-barrier structure with a normal metal interlayer for different temperatures. Solid lines correspond to the clean limit, dotted lines to the dirty limit.

The following comments are important here. First, the distribution  $\rho(D) = (G_N/\pi G_0)D^{-3/2}(1-D)^{-1/2}$  is universal, i.e., independent of the microscopic parameters of the interlayer and has a simple physical meaning: it shows that the electronic transport through the whole two-barrier structure can be considered as a sum over different quantum channels with the transmission coefficient  $D$  and a relative contribution proportional to  $D^{-1/2}(1-D)^{-1/2}$ . Thus, there is equal spectral weight of tunneling ( $D \rightarrow 0$ ) and fully ballistic ( $D \rightarrow 1$ ) channels. This explains why the  $I_C R_N$  product of an SIS'IS junction in the coherent regime lays between the  $I_C R_N$  of a tunnel SIS and a ballistic ScS junctions. Second, this provides the basis for the calculation of the non-stationary current at finite voltage using the formalism of multiple Andreev reflections [105,106]. The  $I-V$  characteristics of  $SI_1S'I_2S$  contacts can be calculated numerically by the integration of the single-channel result [105,106] over the distribution  $\rho(D)$ . This work is presently in progress.

## 5. Experimental results

Double-barrier SINIS junctions have recently been fabricated for potential electronic applications by several groups [11–25]. The details of the fabrication process and achieved parameters are the following.

### 5.1. Fabrication processes

The first experimental observation of a measurable proximity effect through a double-barrier tunnel structure, Nb/Al/AIO<sub>x</sub>/Al/AIO<sub>x</sub>/Nb, was reported in Ref. [11]. The base electrode of the studied structures consisted of 100 nm Nb and 10 nm Al deposited on *R*-plane sapphire substrates. After oxidation in 10 Pa of pure oxygen for 6 min in the deposition system and a pump-down period of 2 h to remove the oxygen, the Al interlayer film with thickness 2–8 nm was deposited and oxidized under the same conditions. Finally, 5 nm Al and 70 nm Nb were sputtered to form the top electrode. The rotation axis of the substrate holder was centered between the Nb and Al targets. During the deposition of all layers, except for the interlayer Al, the samples were rotated at a constant speed, so that repeated passes under the source build up the complete layers. Devices were fabricated using the standard SNEP [1] processing route with an anodization stage. The cross-section of the junctions was about 70 μm<sup>2</sup>.

In Ref. [12], a 50 mm diameter Si wafer was used as a substrate. The junction structure consisted of a Nb base electrode (200 nm), a lower Al layer (6.8 nm), a lower AIO<sub>x</sub> barrier, a middle Al layer (6.8–13.5 nm), an upper AIO<sub>x</sub> barrier, an upper Al layer (6.8 nm), and a Nb counter electrode (200 nm). Nb and Al layers were deposited by dc sputtering. AIO<sub>x</sub> barriers were formed by thermal oxidation in pure oxygen at room temperature. The oxygen pressure  $P$  and oxidation time  $t$  for the lower and upper barriers were the same. The patterning was made by reactive ion etching (RIE) in CF<sub>4</sub> at pressures 2 Pa for Nb and 0.3 Pa for Al. To define the junction's area, all Al and AIO<sub>x</sub> layers were removed, except at the junction itself. Sputtered SiO<sub>2</sub> films (380 nm) were used as insulation layers between the base electrodes and Nb wiring layer. The cross-section of the junctions was 10 × 10 μm<sup>2</sup>.

In Ref. [13], Nb/Al/AIO<sub>x</sub>/Al/AIO<sub>x</sub>/Nb junctions were fabricated on 50 mm diameter Si wafer using a conventional (SNEP) fabrication process [1] in a load-locked sputtering system with a base pressure of 1 × 10<sup>-6</sup> Pa. The tunnel barriers of the junctions were formed by exposing the Al surface to pure oxygen gas. The phenomenological relationship between critical current density  $J_C$  and the  $Pt$  product

$$J_C \approx 3.2 \times 10^5 \times (Pt)^{-0.5} \text{ A/cm}^2 \quad (40)$$

was used for current predictions. Both barriers were formed under the same conditions, the wafer was fixed on the water cooled substrate. The typical area of the junctions was 3 × 3 μm<sup>2</sup>.

The most intensive technological studies were done in Ref. [14]. Here, the technological process, as established in PTB, for the fabrication of shunted Nb/Al/AIO<sub>x</sub>/Nb tunnel structures had been modified and adapted to the special requirements of the double-barrier structure technology. Thermally oxidized silicon wafers of 76 mm in diameter were used as a substrate. The Nb/Al/AIO<sub>x</sub>/Al/AIO<sub>x</sub>/Nb multilayer was deposited and covered by a thin SiO<sub>2</sub> layer, which further had been used as a mask in a subsequent anodization processes. The SIS'IS contacts were structured by RIE in CF<sub>4</sub> and CHF<sub>3</sub>, anodized up to a voltage of 50 V and etched again. As a result, the Nb base electrode and walls of the multilayer structure were covered by a thin insulating layer composed of Al<sub>x</sub>O<sub>y</sub> and Nb<sub>2</sub>O<sub>5</sub>. After that the SiO<sub>2</sub> layer was deposited to additionally isolate the structure. On the final steps the window was opened in SiO<sub>2</sub> to fabricate the contacts to the upper electrodes.

Practically in all technological processes, the metal films were deposited by sputtering in pure Ar atmosphere. In contrast to that in Ref. [18] the middle Al films were deposited in an Ar + O<sub>2</sub> gas mixture with  $1 \times 10^{-5}$ – $2 \times 10^{-5}$  mTorr of O<sub>2</sub> while keeping the total gas pressure at 2 mTorr during the sputtering of the Al. As we shall see below, this does not only influence the transport properties of the Al interlayer making it more “dirty”, but also leads to an increase in the critical temperature of Al. It can be as large as 2–2.3 K [11,18].

Summarizing the description of the fabrication processes, we can conclude that the only difference between the well developed SNEP process for SIS junction fabrication and for double-barrier structures is the need for the additional deposition of an interlayer and an extra barrier, and consequently a longer etching time of the thin Al interlayer in the multilayer patterning process. Etching stage and, especially, the anodization process on the next step of the fabrication process often cause deteriorations of the materials in the vicinity of the surfaces of the multilayer stack. This drawback of the SNEP process makes the properties of the tunnel junctions spatially inhomogeneous because of degraded areas along the junction perimeter. These areas limit the cross-section of the junctions, since the smaller the junctions the larger is the contribution to the junction characteristics from the deteriorated areas of the structure and, hence, the larger is the spread of the junction parameters. In double-barrier devices this drawback is not as essential as it is for the SIS junctions. Large coherence length of the Al interlayer provides effective averaging of the junction properties in the direction perpendicular to the current flow, thus, making the device more technological even than SIS structures.

## 5.2. Uniformity of the junction parameters

The studies [12–14] have confirmed that double-barrier structures are very technological. It means that the junctions are intrinsically uniform. The behavior of their critical current in an external magnetic field  $B$  demonstrates practically ideal Fraunhofer-type diffraction patterns [12,15]. A typical example of an  $I_C(H)$  dependence is shown in Fig. 4. A full suppression of  $I_C$  at the minima was found for junctions with  $J_C \leq 15$  kA/cm<sup>2</sup> and suppression up to 3% of the zero field critical current has been found [13] for the structures with  $J_C \approx 49$  kA/cm<sup>2</sup>. This implies that the current transport is uniform across the barriers and is not dominated by pinholes.

On-chip uniformities of  $I_C$  were studied in Ref. [12] on a 50 mm wafer by fabrication of six junctions in one line with a distance 7.1 mm between the junctions. The maximum to minimum variation for a low- $J_C$  wafer ( $P = 0.67$  Pa,  $t = 300$  s,  $J_C = 0.112$  kA/cm<sup>2</sup>) was  $\pm 4\%$  and that for high- $J_C$  wafer ( $P = 0.40$  Pa,  $t = 150$  s,  $J_C = 6.56$  kA/cm<sup>2</sup>) was 13%.

In Ref. [13], it was shown that in a series connection of 64 Josephson junctions of  $10 \times 10$  μm<sup>2</sup> size and with  $d_{Al} = 5$  nm, fabricated under  $Pt = 100$  Pa s the measured  $J_C$  was 2.8 kA/cm<sup>2</sup> and the spread of  $I_C$  was  $\pm 1.2\%$ . Fig. 5 demonstrates the CVC of this structure. Strong synchronization of the junctions in the array proved their applicability for superconducting integrated circuits.

Finally, in Refs. [14–17], it was shown that the PTB process permitted to fabricate as much as 8192 SIS'IS Josephson junctions in one run on one wafer with a spread in the critical current of about 5% (at  $6\sigma$ ).

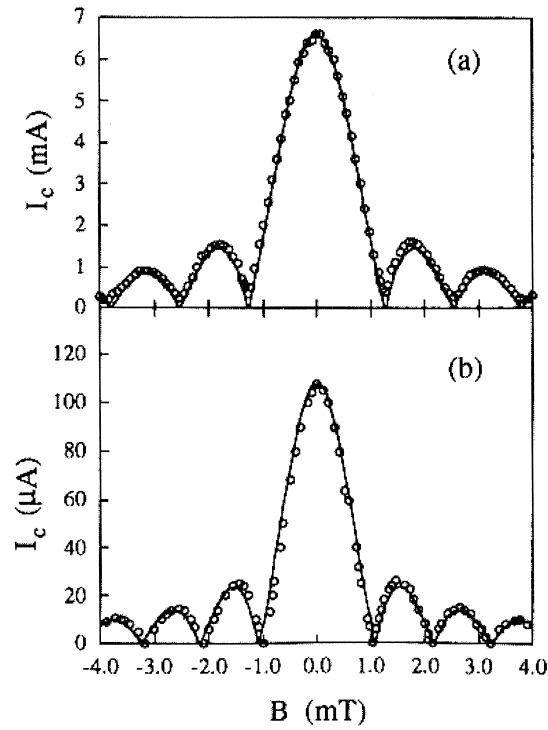


Fig. 4. The magnetic field dependence [12] of  $I_c$  of Nb/ $\text{AlO}_x$ /Al/ $\text{AlO}_x$ /Nb junctions with 9.5 nm middle Al layer at  $T = 4.2$  K. The size of the junctions is  $10 \times 10 \mu\text{m}^2$ . Critical current density for the samples (a) and (b) is 6.56 and 0.112 kA/cm<sup>2</sup> correspondingly. Open circles represent experimental data and solid lines are the theoretical predictions,  $I_c(B) = I_c(0)\sin(\pi B/B_0)/(\pi B/B_0)$ , where  $B_0 =$  (a) 1.27 mT and (b) 1.08 mT.

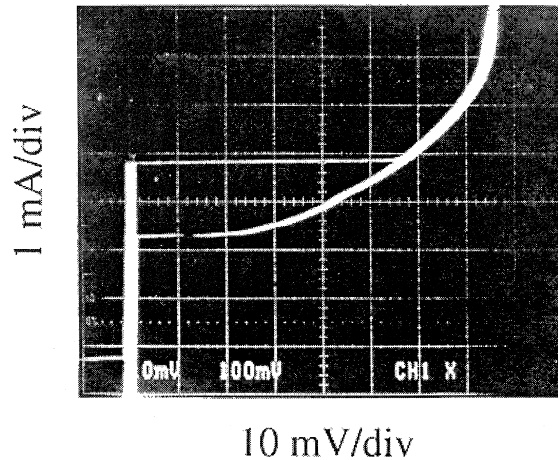


Fig. 5. CVC for 64 double-barrier junctions connected in series from Ref. [13]. Junction size is  $10 \times 10 \mu\text{m}^2$ , thickness of Al interlayer is 5 nm, critical current density of the devices is 2.8 kA/cm<sup>2</sup>, and the spread of  $I_c$  is  $\pm 1.2\%$ .

### 5.3. Electrical parameters of double-barrier structures

CVCs of double-barrier devices have a form close to the RSJ type with a small hysteresis in the low voltage region. Typical CVC are shown in Fig. 6a. Fig. 6b shows hystereses as a function of  $J_C$ . The magnitude of hysteresis is characterized by the ratio  $I_R/I_C$ , where  $I_R$  is the reset current at which the junctions return from a voltage state to a zero voltage state. It can be seen that the hysteresis is suppressed by increasing the critical current density or the thickness of the interlayer.

The electrical parameters of fabricated junctions are summarized in Table 2. It follows that reasonable values of the  $I_C R_N$  product can be achieved already at present in junctions with a critical current density larger than 1 kA/cm<sup>2</sup>.

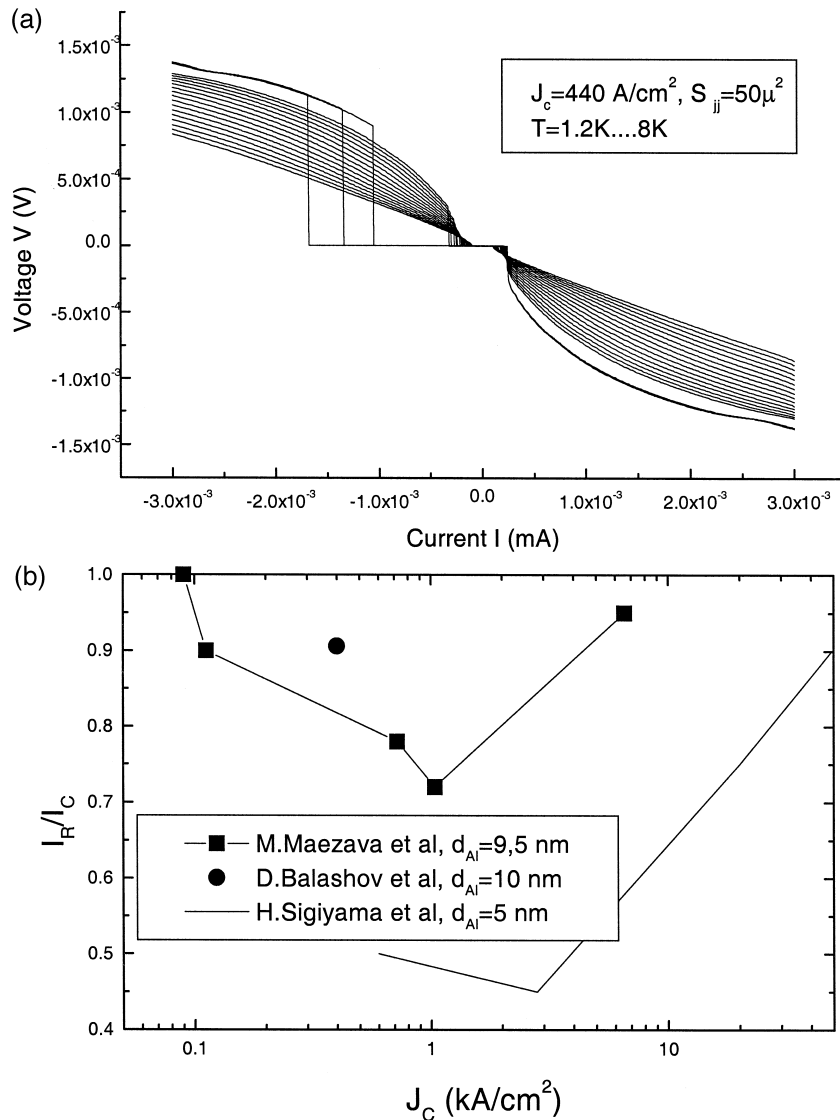


Fig. 6. (a) Typical CVC of a double-barrier Josephson junction, from Ref. [14], (b) dependence of the reset current on the critical current density of the junctions [12–14].

Table 2  
Parameters of SIS'IS double-barrier structures at  $T = 4.2$  K

Sample	$d_{\text{Al}}$ (nm)	$Pt$ (Pa s)	$J_C(4.2)$ (A/cm <sup>2</sup> )	$R_B$ ( $\mu\Omega$ cm <sup>2</sup> )	$I_C R_N$ (mV)
A [12]	6.8	0.4	1040	0.11	0.11
B [12]	9.5	0.4	6560	0.036	0.24
C [12]	9.5	0.4	720	0.087	0.062
D [12]	9.5	0.67	112	0.28	0.031
E [12]	13.5	0.67	90	0.2	0.018
A [13]	0	300	9000	–	–
B [13]	0.3	300	1200	–	–
C [13]	0.5	300	800	–	–
D [13]	1	300	400	0.2	0.08
E [13]	3	300	400	0.2	0.08
F [13]	5	300	700	0.2	0.14
A [14]	8	24	1100	0.225	0.25
B [14]	8	48	350	0.4	0.14
C [14]	8	72	140	0.62	0.088
D [14]	8	96	75	0.81	0.061
E [14]	8	120	35	1.28	0.057
A [18]	6.6	–	17	0.7	0.012
A [11]	2.2	3600	90	0.5	0.045
A [11]					

Several independent factors are influencing the value of the  $I_C R_N$  product. They are

- transparency of the interfaces;
- thickness of the interlayer  $S'$  material;
- critical temperature of the  $S'$  metal;
- proximity effect in the composite Nb/Al electrodes.

To develop a stable technology for large-scale integrated circuits, the systematic study of the influence of all these factors on the junction parameters must be done. This program is not complete yet. The existing data will be discussed below.

### 5.3.1. Transparency of the interfaces

The transparency of interfaces is the main parameter influencing  $J_C$  and the form of the  $I$ – $V$  curves. In classical SIS Josephson devices an increase of the interface transparency is accompanied by the formation of pin holes in the barrier and degradation of the reproducibility of the technological parameters. As was shown in Ref. [95], increase in the critical current density from 1 to 10 kA/cm<sup>2</sup> results in a systematic increase in the subgap leakage current, appearance of a strong subharmonic gap structure and of an excess current on CVC. All these effects are consistent with Andreev reflections in the high transmittance regions of the barrier. To provide larger  $J_C$ , it would be necessary to fabricate a barrier with an average thickness less than one atomic unit cell of aluminum oxide. In this case, the dielectric layer is not uniform anymore and the tunneling current is flowing parallel to the supercurrent across the holes in the barrier [107].

In contrast, the double-barrier structure with critical current densities as large as 49 kA/cm<sup>2</sup> demonstrated very good uniformity of the supercurrent distribution [13]. There are at least two reasons for that. First, the intermediate Al has a large coherence length and it effectively averages the transport properties of the double-barrier structure in the planes parallel to the directions of the current flow. The larger the concentration  $N_C$  of the constrictions, the more effective is this self averaging and the more homogeneous is the superconducting state in the interlayer. Simple estimations show that the spatial variations of the superconducting correlation, induced via pin holes of a diameter  $a \ll \xi_{\text{nd}}^*$ ,  $d$  into the normal metal with a thickness of  $d \ll \xi_{\text{nd}}^*$ , decay at a

distance of  $(a\xi_{nd}^*)^{1/2}$ . The increase of the barrier transparencies up to a level accompanied by the formation of pin holes will not lead to large spread of the parameters if  $(a\xi_{nd}^*)^{1/2} \ll d$ .

In the limit of small  $N_C$ , simple geometrical arguments are valid. In this case, the probability for the propagation of electrons across two pin holes located at different barriers, is proportional to the very small factor  $(a^2/S)^2$ , where  $a$  is the effective radius of a constriction and  $S$  is the junction area. A constriction located only in one of the barriers provides the correction to the probability distribution function (39) proportional to  $(a^2/S)$ . One can show that this should not change the average supercurrent in the practically important regime of small values of  $\gamma_{eff}$ . Indeed, in this regime, the critical current per channel is proportional to the transparency  $D$  of the individual interface (see Eq. (37)), while the contribution of the pin hole to  $J_C$  is also proportional to  $D$  due to the presence of the second barrier. Given the smallness of the pin hole channel fraction  $(a^2/S)$ , one should expect small corrections to the critical current from these channels. In contrast to that, in single-barrier high- $J_C$  SIS junctions, the contribution from a pin hole to the net current is controlled by channels with  $D = 1$  and thus exceeds by orders of magnitude the direct tunneling contribution, which is proportional to  $D \ll 1$ .

These simple arguments provide the opportunity to perform more weak oxidation of the interfaces compared to the one in standard SIS junctions technology and achieve, if necessary, the level of 10–100 kA/cm<sup>2</sup> without degradation of the junction parameters.

The study [13] of the  $J_C(Pt)$  dependence of SIS/IS junctions with a 5 nm thick intermediate Al layer gives (see Fig. 7) that in contrast to the law obtained for conventional trilayer junctions (40),  $J_C$  exponentially decreases for  $Pt$  product  $< 100$  Pa s

$$J_C \approx J_{C0} \exp\left\{-\frac{Pt}{11}\right\}, \quad J_{C0} \approx 415 \text{ kA/cm}^2, \quad (41)$$

while  $J_C$  hardly changes for  $Pt$  product  $> 100$  Pa s. The parameter values may vary from laboratory to laboratory due to different oxidation circumstances (for example the vapor background pressure). The scaling obtained for SIS junctions (40) is still valid around  $Pt \approx 100$  Pa s, indicating that the conduction mechanism through the barriers is unchanged. Unfortunately, the lack of experimental data does not permit us to estimate the values of the suppression parameters in this experiment.

Fig. 8 provides the most straightforward way for such an estimation. It contains the theoretical  $V_C(\gamma_{eff})$  dependencies calculated from Eq. (9) for  $T_C^* = 1.25$  K and for different temperatures. To define  $\gamma_{eff}$ , it is enough to extract from the data from Ref. [14] the ratio  $(I_C R_N)/(2\pi T_C)$  and plot the points on the curve corresponding to the working temperature. Following this procedure (see Fig. 8), we have found the value of the suppression parameter  $\gamma_{eff} \approx 100$  for junctions with  $J_C \approx 1$  kA/cm<sup>2</sup>.

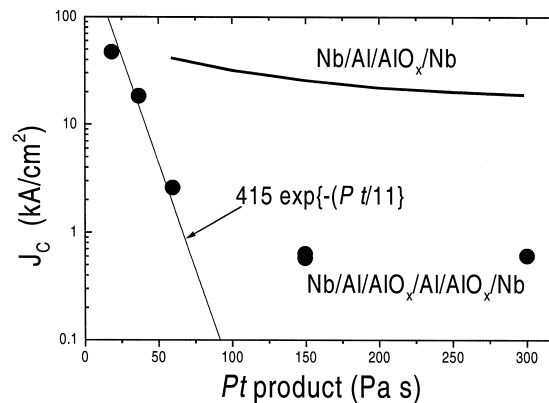


Fig. 7. Dependence of the critical current density of the double-barrier devices with a thickness of the intermediate Al layer 5 nm as a function of the  $Pt$  product [13]. The solid line indicates  $J_C$  of the conventional trilayer SIS junction with the relationship  $J_C \propto (Pt)^{-0.5}$ . The dashed line corresponds to  $J_C \approx J_{C0} \exp\{-Pt/11\}$ , where  $J_{C0} \approx 415$  kA/cm<sup>2</sup>.

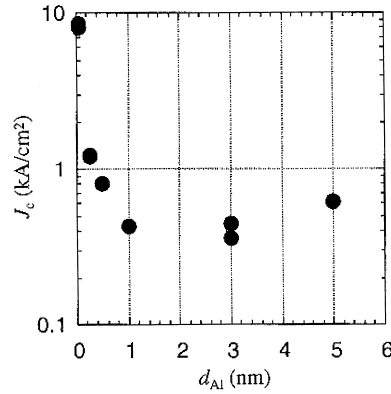


Fig. 8. Critical current density of the double-barrier devices as a function of the thickness of the interlayer materials in accordance with the results of Ref. [13].

On the other hand, the transparency of the Nb/Al interfaces in the composite bottom and top electrodes SS'IS'IS'S junctions is also finite and corresponds to a suppression parameter close to 1 [92,93]. This means that in order to locate all processes in the middle layer, it is reasonable to have the suppression parameter of  $\gamma_{\text{eff}} \approx 10$ . With this value, as follows from Fig. 8, the  $I_C R_N$  product at 4.2 K will only be four times smaller than in an ideal SIS junction. To our mind, this is rather close to reality, especially if we take into account that there was at least one realization of a double-barrier device of that type [12].

### 5.3.2. Influence of the thickness of the S' interlayer material on the junctions parameters

To understand the reasons for degradation of the  $I_C R_N$  product with the increase of the thickness  $d$  of the interlayer material, we will suppose first that  $d$  is negligibly small. Thus, we have at the beginning SIS tunnel junctions. In symmetric tunnel structures, the real part of quasiclassical Green's function is constant across the interface  $\text{Re}\Phi = f \cos(\varphi/2)$ , while the imaginary part changes discontinuously across the barrier  $\text{Im}\Phi \propto xDf \times \sin(\varphi/2) \propto R_B^{-1} f \sin(\varphi/2)$ . Since the supercurrent is proportional to the  $\text{Re}\Phi \text{Im}\Phi'$  product, the characteristic voltage appears to be independent of the barrier material.

An increase in the interlayer thickness breaks the spatial homogeneity of  $\text{Re}\Phi$  and at  $d \gtrsim \xi_{\text{nd}}^*/\gamma_B$  the coupling between the superconducting banks is additionally suppressed because of  $\text{Re}\Phi = \gamma_B^{-1} f \cos(\varphi/2)$ . Using the empirical relation between the Al film thickness  $d$  and decay length  $\xi_{\text{nd}}^*$  [92]

$$\xi_{\text{nd}}^* = A_1 \left( 1 - \exp\left\{ -\frac{d}{d_1} \right\} \right) + A_2 \left( 1 - \exp\left\{ -\frac{d}{d_2} \right\} \right) \quad (42)$$

where  $A_1 = 69.1$  nm,  $A_2 = 116.5$  nm,  $d_1 = 11.7$  nm,  $d_2 = 97.8$  nm for  $d \lesssim 10$  nm we approximately have  $\xi_{\text{nd}}^* \approx 7d$ . Combining this estimate with the condition  $d \gtrsim \xi_{\text{nd}}^*/\gamma_B$  we find that the transition to the devices with degraded  $I_C R_N$  product starts from  $\gamma_B \gtrsim 10$ .

From the typical value of the specific boundary resistance (see Table 2)  $R_B \approx 0.1 \mu\Omega \text{ cm}^2$  and transport constants of thin Al films [92] at 4.2 K

$$\rho_{\text{Al}}(d \approx 10 \text{ nm}) \approx 10 \mu\Omega \text{ cm}, \quad \xi_{\text{nd}}^*(d \approx 10 \text{ nm}) \approx 70 \text{ nm}$$

for the suppression parameter at the SIS' interface of SIS'IS junctions we have  $\gamma_B \approx 1000$ . Taking into account that  $d/\xi_{\text{nd}}^* \approx 0.1$ , we finally arrive at the typical experimental value of a suppression parameter  $\gamma_{\text{eff}}$  of about 100. This value is just in the range of the scope of experimental results [13,14]. This simple analysis has an experimental confirmation [13].

It was shown in Ref. [13] that in double-barrier devices with  $d_{\text{Al}} \lesssim 1$  nm,  $J_C$  decreases drastically (see Fig. 8) with an increase in  $d_{\text{Al}}$ , while the CVC of the junctions were almost the same as those of the trilayer junctions.

This means that the first  $\text{AlO}_x$  surface is not completely covered with a second Al film. Thus, there is a formation of the SIS and SIS'IS junctions in parallel. The area occupied by SIS'IS structures is relatively small, so that the characteristics of the junction reflect those of the SIS Josephson devices.

For  $d_{\text{Al}} \gtrsim 1$  nm, the second Al film covers the first  $\text{AlO}_x$  surface perfectly. The critical current density is practically independent of  $d_{\text{Al}}$  and controlled only by interfaces. On the CVC, there is a current deficit at large voltage  $V \gtrsim 3$  mV typical for double-barrier devices and the hysteresis at small voltages is effectively suppressed.

### 5.3.3. Influence of the critical temperature of the $S'$ metal

It follows from the theoretical consideration given above that one might expect an enhancement of the  $I_C R_N$  product in the vicinity of the critical temperature of the interlayer metal. Usually, the temperature of superconducting transition for Al is close to 1.3 K and experimental data (see Fig. 9) really demonstrate such an enhancement. The best fit of the data [10] by theoretical curves were achieved at  $T_C^* = 1.25$  K and  $\gamma_{\text{eff}} \approx 2000$ . It is important to note that in the technological process from Ref. [14] the oxidation and deposition of Al were performed in different chambers. Samples can be transported between them without breaking the vacuum. This results in lower  $\gamma_{\text{eff}} \approx 100$ .

In contrast, in Refs. [11,18], the oxidation and deposition processes occurred in the same chambers. As a result, the intermediate Al was effected by the residual oxygen during the deposition. This results in an increase in the critical temperature of Al to the values  $T_C^* \approx 2.0$ – $2.3$  K. Fig. 10 shows a fit of the data [18] within the developed theory for the dirty limit. Good agreement has been found for  $T_C^* \approx 2.7$  and  $\gamma_{\text{eff}} \approx 1600$ .

Thus, the increase of  $T_C^*$  of the interlayer, for example, by using the combination of thin Al and Nb layers as complex interlayer material can provide in principle the possibility for enhancing the  $I_C R_N$  product without a noticeable change in the  $\sin \varphi$  current–phase relation.

### 5.3.4. Influence of the proximity effect in the composite Nb/Al electrodes

A degradation of the critical current density in double-barrier devices can also take place due to the proximity effect in composite Nb/Al bottom and top electrodes. This problem was intensively studied in Refs. [92,93,98].

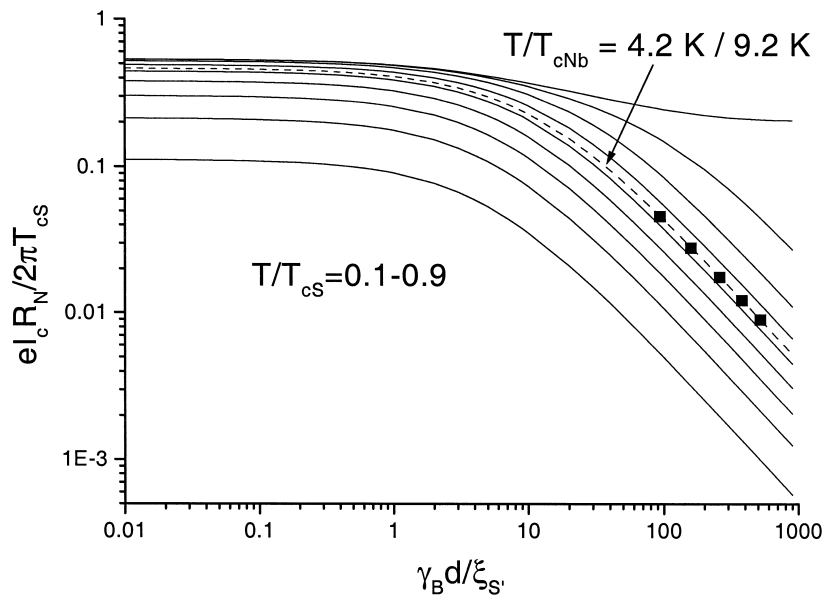


Fig. 9. Solid lines are theoretical  $V_C(\gamma_{\text{eff}})$  dependences calculated from Eq. (9) for  $T_C^* = 1.25$  K and different temperatures. Filled circles are the experimental data from Ref. [14].

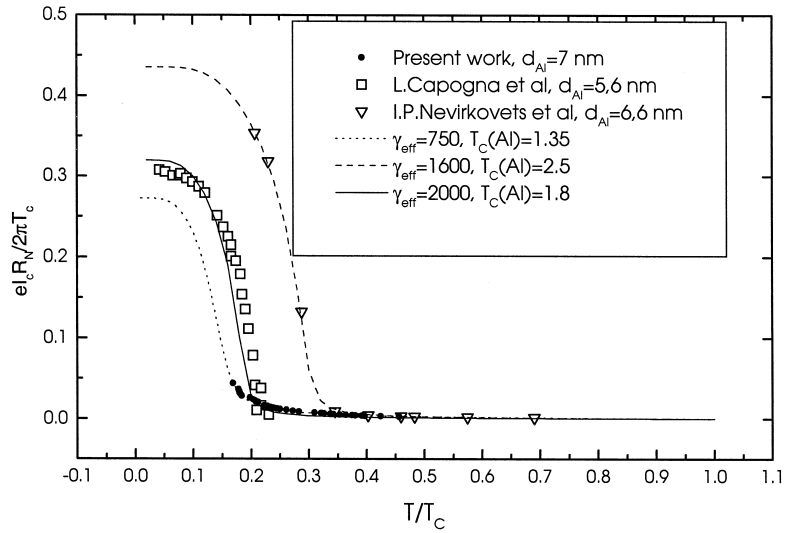


Fig. 10. Comparison of temperature dependences of  $I_C R_N$  product calculated from Eq. (9) for  $T_C^* = 1.25$  K and various values of  $\gamma_{\text{eff}}$  with the experimental data from the present work and Refs. [11,18].

It was shown that typical values of the suppression parameters  $\gamma$  and  $\gamma_B$  at Nb/Al interfaces are in the range  $\gamma \lesssim 0.2$ ,  $\gamma_B \lesssim 1$ . Fig. 11 shows the temperature dependence of the double-barrier critical current as a function of suppression parameter  $\gamma$  and  $\gamma_B = 0$ , calculated in the framework of the dirty limit model. It is clearly seen that in the practically interesting temperature interval, suppression of the critical current does not exceed 10%, even for relatively large  $\gamma = 0.2$ .

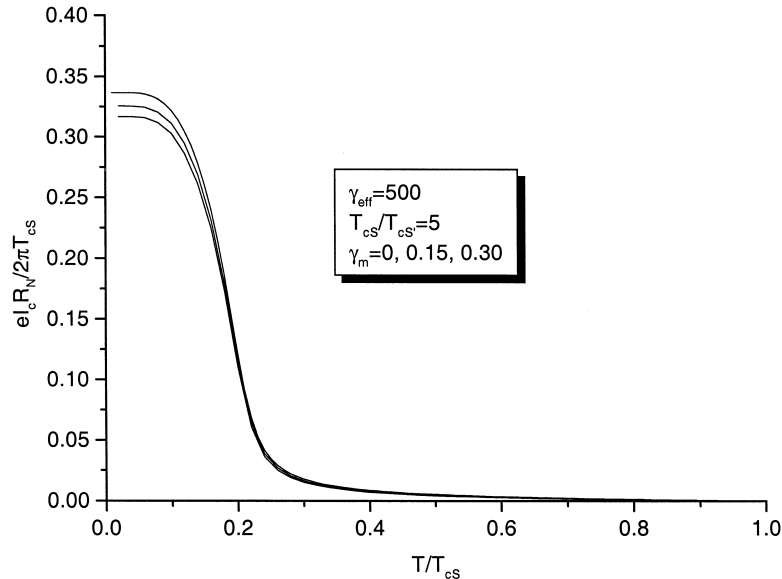


Fig. 11. Temperature dependences of the critical current in a double-barrier junction as a function of the suppression parameters  $\gamma_m$  and  $\gamma_B = 0$ , characterizing the proximity effect in the composite Nb/Al electrode, calculated in the framework of the Usadel equations. In the practically interesting temperature interval the suppression of the critical current does not exceed 10% even for relatively large  $\gamma_m = 0.3$ .

Recently, an effective method of planarization of the base electrode [93] was proposed. In contrast to the standard SNEP process, it gives the possibility to get an oxidized Al film as thin as 3–4 nm, which is twice smaller than in the standard technology. As a result, the proximity effect is practically eliminated from the bottom electrode. The density of states near the interface becomes very close to the BCS form, the knee structure on CVC completely disappears and the leakage current is effectively suppressed.

We believe that the bottom electrode planarization should be effectively used during fabrication of the double-barrier structures. This does not only eliminate the degradation of the junction parameters due to the proximity effect in the electrode, but also makes the morphology of all interfaces better providing the possibility for using thinner Al or a Nb/Al composite as the interlayer.

## 6. Non-stationary effects in double-barrier devices

Non-stationary and non-equilibrium effects in double-barrier devices are intensively studied in the last few years (see Refs. [9,108a,108b,109] and references therein). From this study, it follows that important knowledge about the values of the suppression parameters can be extracted from the examination of the conductance of the double-barrier structures with one superconducting electrode. It was shown that the CVC of SIN'IN structures has the form

$$I = \frac{1}{2R_N} \int_0^\infty D(\varepsilon) \left[ \tanh\left(\frac{\varepsilon + eV}{2T}\right) - \tanh\left(\frac{\varepsilon - eV}{2T}\right) \right] d\varepsilon, \quad (43)$$

$$R_N = R_{B1} + R_{B2} + R.$$

Here,  $R$ ,  $R_{B1}$  and  $R_{B2}$  are the resistances of normal interlayer and the barriers correspondingly. The effective diffusion coefficient  $D(\varepsilon)$  was calculated in Refs. [108a,108b,109] in various limits.

In the practically interesting case of large boundary resistance

$$R_{B1}, R_{B2} \gg R \quad \text{or} \quad \gamma_{B1}, \gamma_{B2} \gg \frac{d}{\xi_{nd}^*} \quad (44)$$

in the zero voltage limit, it was found that

$$\sigma_d(0) = \frac{1}{4TR_N} \int_0^\infty D(\varepsilon) \cosh^2\left(\frac{\varepsilon}{2T}\right) d\varepsilon = \frac{R_{B1}R_{B2}}{(R_{B1}^2 + R_{B2}^2)^{3/2}}, \quad (45)$$

while in the large voltage limit

$$\sigma_d(V \gg \Delta/e) = \frac{1}{R_{B1} + R_{B2}}. \quad (46)$$

From Eqs. (45) and (46), it follows that independent measurements of zero and large voltage conductances open the direct way of estimating the individual interface boundary resistances and, hence, the suppression parameters of the boundaries.

Additional information about the interface resistance can also be extracted from the value of the current deficit  $I_{\text{def}}$  which in NIN'IS structures always exists at large voltages [108a,108b,109]. In the practically

interesting case  $\gamma_{B1}, \gamma_{B2} \gg \xi_{nd}^*/d$ , current deficit depends on the ratio of the interface resistance  $R_{NN'}$ ,  $R_{SN'}$  and the value of the order parameter in the electrodes.

$$R_n I_{\text{def}} = -\Delta_B J_1(x), \quad x = \frac{R_{NN'}}{R_{SN'}} \quad (47)$$

$$J_1(x) = \theta(x-1) \frac{2x \operatorname{atanh}\left(\sqrt{(x-1)/(x+1)}\right)}{(x-1)\sqrt{x^2-1}} + \theta(1-x) \frac{2x \operatorname{atan}\left(\sqrt{(1-x)/(x+1)}\right)}{(x-1)\sqrt{1-x^2}} + \frac{1}{(x-1)},$$

In the limits of large and small  $x$ , the function  $J_1(x)$  is reduced to 1 and  $(\log(2x) - 1)/x$ , respectively, while  $J_1(1) = 2/3$ .

Therefore, the experimental study of the details of CVC provides the possibility to get information about the suppression parameters.

## 7. Conclusion

Summarizing the discussion, we can conclude that among the possible candidates for the key elements in large-scale superconducting microcircuits (HTS Josephson junctions, LTS SNS weak links, high- $J_C$  tunnel SIS structures, double-barrier SS'IS'IS'S devices) only double-barrier junctions can, in the nearest future, open the way to practical devices. There are several arguments supporting this conclusion.

(1) These structures can be fabricated, making use of a small modification of the standard SNEP fabrication process.

(2) Their parameters are intrinsically homogeneous on the individual level due to additional averaging of the irregularities of the interface transparency by the intermediate Al layer, which is characterized by a large coherence length. They are reproducible on the on-chip level. This fact was successfully demonstrated by several technological groups.

(3) Their CVC are very close to the form predicted by the RSJ model. This makes the dynamical processes sufficiently more simple compared to high- $J_C$  tunnel SIS structures.

(4) Even at the present level ( $J_C \approx 1 \text{ kA/cm}^2$ ,  $\gamma_{\text{eff}} \approx 100$ ), these structures provide an  $I_C R_N$  product close to 0.25 mV. We believe that these parameters can be improved at least four times resulting in  $I_C R_N \approx 1 \text{ mV}$ , ( $J_C \approx 10\text{--}20 \text{ kA/cm}^2$ ,  $\gamma_{\text{eff}} \approx 10$ ), without visible deviation from the RSJ-type CVC.

(5) Possibilities for injection of the supercurrent into the intermediate S' layer of SS'IS'IS'S junctions open the way to tunable Josephson devices.

(6) Even now, there are several examples of RSFQ devices and chips for the Josephson voltage standard fabricated on the basis of double-barrier Josephson structures, which have demonstrated good performance.

It is also necessary to point out that there are a set of new physical effects in double-barrier junctions, which still remain to be solved both theoretically and experimentally.

## Acknowledgements

This work was supported in part by INTAS (project INTAS-97-1712) and ISTC (project 1197). The authors thank D. Balashov, A. Braginskii, F.-Im. Buchholz, J. Flokstra, G. Gerritsma, M.I. Khabipov, H. Kohlstedt, V.P. Koshelets, I.P. Nevirkovets, J. Niemeyer, V.K. Semenov and H. Schulze for stimulating discussions and exchange of experimental results.

## References

- [1] M. Gurwitsch, W.A. Washington, H.A. Huggins, *Appl. Phys. Lett.* 42 (1983) 472.
- [2] K.K. Likharev, V.K. Semenov, *IEEE Trans. Appl. Supercond.* 1 (1991) 3.
- [3] C.A. Hamilton, C.J. Burroughs, R.L. Kauts, *IEEE Trans. Instrum. Meas.* 44 (1995) 233.
- [4] N. Schulze, F. Muller, R. Behr, J. Kohlmann, J. Niemeyer, D. Balashov, Abstracts of ASC-98, *IEEE Trans. Appl. Supercond.* (1999) to be published.
- [5] V.P. Koshelets, S.V. Shitov, A.V. Shchukin, L.V. Filippenko, P.V. Dmitriev, V.L. Vaks, J. Mygind, A.M. Baryshev, W. Luinge, H. Golstein, Proc. of ASC-98 Conference, Report EQB-04, *IEEE Trans. Appl. Supercond.*, 1999.
- [6] V.P. Koshelets, S.V. Shitov, L.V. Filippenko, V.L. Vaks, J. Mygind, A.M. Baryshev, W. Luinge, N. Whyborn, External Phase Locking of 270–440 GHz Josephson Flux Flow Oscillator. Preprint, 1999.
- [7] W. Chen, A.V. Rylyakov, V. Patel, J.E. Lukens, K.K. Likharev, *Appl. Phys. Lett.* 73 (1998) 2817.
- [8] M.Yu. Kupriyanov, V.F. Lukichev, *Sov. Phys. JETP* 67 (1988) 1163.
- [9] A.V. Zaitsev, *Physica C* 185–189 (1991) 2539.
- [10] A. Brinkman, A.A. Golubov, M.Yu. Kupriyanov, H. Rogalla, submitted to *Phys. Rev. B*.
- [11] L. Capogna, M.G. Blamire, *Phys. Rev. B* 53 (1996) 5683.
- [12] M. Maezawa, A. Shiji, *Appl. Phys. Lett.* 70 (1997) 3603.
- [13] H. Sugiyama, A. Yanada, M. Ota, A. Fujimaki, H. Hayakawa, *Jpn. J. Appl. Phys.* 36 (1997) L1157.
- [14] D. Balashov, F.-Im. Buchholz, H. Schulze, M.I. Khabipov, W. Kessel, J. Niemeyer, *Supercond. Sci. Technol.* 11 (1998) 1401.
- [15] N. Schulze, R. Behr, F. Muller, J. Niemeyer, *Appl. Phys. Lett.* 73 (1998) 996.
- [16] R. Behr, N. Schulze, F. Muller, J. Kohlmann, J. Niemeyer, *IEEE Trans. Instrum. Meas.* (1999) to be published.
- [17] M.I. Khabipov, D. Balashov, F.-Im. Buchholz, W. Kessel, J. Niemeyer, RFSQ Circuitry Realised in SINIS Technology Process. Preprint, 1999.
- [18] I.P. Nevirkovets, J.B. Ketterson, S. Lomatch, *Appl. Phys. Lett.* 74 (1999) 1624.
- [19] I.P. Nevirkovets, T. Doderer, A. Laub, M.G. Blamire, J.E. Evetts, *J. Appl. Phys.* 80 (1996) 2321.
- [20] I.P. Nevirkovets, J.E. Evetts, M.G. Blamire, Z.H. Barber, E. Goldobin, *Phys. Lett. A* 232 (1997) 299.
- [21] I.P. Nevirkovets, *Phys. Rev. B* 56 (1997) 832.
- [22] I.P. Nevirkovets, *Supercond. Sci. Technol.* 8 (1995) 575.
- [23] H. Amin, M.G. Blamire, J.E. Evetts, *IEEE Trans. Appl. Supercond.* 3 (1993) 2204.
- [24] L. Capogna, G. Burnell, M.G. Blamire, *IEEE Trans. Appl. Supercond.* 7 (1997) 2415.
- [25] P.V. Komissinski, G.A. Ovsyannikov, *Phys. Rev. B* 54 (1996) 13184.
- [26] G.E. Babayan, L.V. Filippenko, G.A. Ovsyannikov, O.V. Uvarov, V.P. Koshelets, *Supercond. Sci. Technol.* 4 (1991) 476–478.
- [27] Z.G. Ivanov, V.K. Kaplunenko, E.A. Stepantsov, E. Wikborg, T. Cleason, *Supercond. Sci. Technol.* 7 (1994) 239.
- [28] V.K. Kaplunenko, Z.G. Ivanov, E.A. Stepantsov, T. Cleason, E. Wikborg, *Appl. Phys. Lett.* 67 (1995) 282.
- [29] V.K. Kaplunenko, Z.G. Ivanov, E.A. Stepantsov, T. Cleason, T. Horst, Z.J. Sun, R. Kromann, Y.Q. Shen, P. Vase, T. Freltoft, E. Wikborg, *Appl. Phys. Lett.* 67 (1995) 138.
- [30] S. Shokhor, B. Nadgorny, M. Gurvitch, V.K. Semenov, Yu. Polyakov, K.K. Likharev, Y. Hou, J.M. Phillips, *Appl. Phys. Lett.* 67 (1995) 2869.
- [31] B. Oelze, B. Ruck, M. Roth, R. Domel, M. Siegel, A.Yu. Kidiyarova-Shevchenko, T.V. Filippov, M.Yu. Kupriyanov, G. Hildebrandt, H. Topfer, F.H. Uhlmann, W. Prusseit, in: D. Dew-Hughes (Ed.), *Applied Superconductivity 1995*. Inst. Phys. Conf. Ser. N148, Bristol, 1995, p. 1701.
- [32] M.G. Forrester, J.X. Przybysz, J. Talvacchio, J. Kang, A. Davidson, J.R. Gavaler, *IEEE Trans. Appl. Supercond.* 5 (1997) 3401.
- [33] B. Oelze, B. Ruck, M. Roth, R. Domel, M. Siegel, A.Yu. Kidiyarova-Shevchenko, V. Filippov, M.Yu. Kupriyanov, G. Hildebrandt, H. Topfer, F.H. Uhlmann, W. Prusseit, *Appl. Phys. Lett.* 68 (1996) 2732.
- [34] B. Oelze, B. Ruck, E. Sodtke, A.F. Kirichenko, M.Yu. Kupriyanov, W. Prusseit, *Appl. Phys. Lett.* 70 (1997) 658.
- [35] B. Oelze, B. Ruck, E. Sodtke, T. Filippov, A.Yu. Kidiyarova-Shevchenko, M. Kupriyanov, W. Prusseit, *IEEE Trans. Appl. Supercond.* 7 (1997) 3450.
- [36] B. Ruck, B. Oelze, R. Dittmann, A. Engelhardt, E. Sodtke, W.E. Booij, M.G. Blamire, *Appl. Phys. Lett.* 72 (1998) 2328.
- [37] Y. Chong, B. Ruck, R. Dittmann, C. Horstmann, A. Engelhardt, G. Wahl, B. Oelze, E. Sodtke, *Appl. Phys. Lett.* 72 (1998) 1513.
- [38] J.D. McCambridge, M.G. Forrester, D.L. Miller, B.D. Hunt, J.X. Przybysz, J. Talvacchio, R.M. Young, *IEEE Trans. Appl. Supercond.* 7 (1997) 3622.
- [39] R. Koch, T. Scherer, M. Winter, W. Jutsi, *IEEE Trans. Appl. Supercond.* 7 (1997) 3646.
- [40] M.S. Dilorio, S. Yoshizumi, K.Y. Yang, J. Zhang, M. Maung, *Appl. Phys. Lett.* 58 (1991) 2552.
- [41] R.H. Ono, L.R. Vale, K.R. Kimminau, J.A. Beal, M.W. Cromar, C.D. Reintsema, T.E. Harvey, P.A. Rosenthal, D.A. Rudman, *IEEE Trans. Appl. Supercond.* 3 (1993) 2389.
- [42] P.A. Rosenthal, E.N. Grossman, R.H. Ono, L.R. Vale, *Appl. Phys. Lett.* 63 (1993) 1984.
- [43] C.D. Reintsema, R.H. Ono, T.E. Harvey, N. Missert, L.R. Vale, *Appl. Phys. Lett.* 64 (1994) 637.

- [44] S.J. Berkowitz, W.J. Skocpol, P.M. Mankiewich, R.H. Ono, N. Missert, P.A. Rosenthal, L.R. Vale, *J. Appl. Phys.* 76 (1994) 1337.
- [45] M. Grove, R. Dittmann, M. Bode, M. Siegel, A.I. Braginski, *Appl. Phys. Lett.* 69 (1996) 696.
- [46] M. Bode, M. Grove, M. Siegel, A.I. Braginski, *J. Appl. Phys.* 80 (1996) 6378.
- [47] J. Gao, W.A.M. Aarnink, G.J. Gerritsma, H. Rogalla, *Physica C* 171 (1990) 126.
- [48] J. Gao, Yu.M. Boguslavskij, B.B.G. Klopman, D. Terpstra, R. Wijbrans, G.J. Gerritsma, H. Rogalla, *J. Appl. Phys.* 72 (1992) 575.
- [49] A.A. Golubov, M.A.J. Verhoeven, I.A. Devyatov, M.Yu. Kupriyanov, G.J. Gerritsma, H. Rogalla, *Physica C* 235–240 (1994) 3261.
- [50] M.A.J. Verhoeven, G.J. Gerritsma, H. Rogalla, A.A. Golubov, *Appl. Phys. Lett.* 69 (1996) 848.
- [51] K. Verbist, O.I. Lebedev, G. van Tendeloo, M.A.J. Verhoeven, A.J.H.M. Rijnders, D.H.A. Blank, H. Rogalla, *Appl. Phys. Lett.* 70 (1997) 1167.
- [52] T. Satoh, M. Hidaka, M.Yu. Kupriyanov, J.S. Tsai, *IEEE Trans. Appl. Supercond.* 5 (1995) 2612.
- [53] R. Dommel, C. Horstmann, M. Siegel, A.I. Braginskii, M.Yu. Kupriyanov, *Appl. Phys. Lett.* 67 (1995) 1775.
- [54] J. Yoshida, T. Nagano, T. Hashimoto, *J. Low Temp. Phys.* 106 (1997) 327.
- [55] J.G. Wen, N. Koshizuka, C. Traeholt, H.W. Zandbergen, E.M.C.M. Reuvekamp, H. Rogalla, *Physica C* 255 (1995) 293.
- [56] G.J. Gerritsma, M.A.J. Verhoeven, R. Moerman, D.H.A. Blank, H. Rogalla, *J. Alloys Compd.* 251 (1997) 196.
- [57] C. Horstmann, P. Leinenbach, A. Engelhardt, R. Dittmann, U. Memmert, A.I. Braginski, J.L. Jia, R. Gerber, U. Hartmann, *Physica C* 302 (1998) 176.
- [58] T. Satoh, M. Hidaka, S. Tahara, *IEICE Trans Electron.* 81 (1998) 1532.
- [59] C. Horstmann, P. Leinenbach, R. Dittmann, U. Memmert, U. Hartmann, A.I. Braginski, *IEEE Trans. Appl. Supercond.* 7 (1997) 2844.
- [60] A.A. Golubov, V.M. Krasnov, M.Yu. Kupriyanov, *J. Low Temp. Phys.* 106 (1997) 249.
- [61a] A.A. Golubov, M.Yu. Kupriyanov, *Zh. Eksp. Teor. Fiz.* 105 (1994) 1442.
- [61b] A.A. Golubov, M.Yu. Kupriyanov, *JETP* 78 (1994) 777.
- [62] M.Yu. Kupriyanov, *J. Low Temp. Phys.* 106 (1997) 149.
- [63a] M.Yu. Kupriyanov, K.K. Likharev, *Uspekhi Fiz. Nauk.* 160 (1990) 49.
- [63b] M.Yu. Kupriyanov, K.K. Likharev, *Sov. Phys. Uspekhi* 33 (1990) 340.
- [64a] I.A. Devyatov, M.Yu. Kupriyanov, *Zh. Eksp. Teor. Fiz.* 104 (1993) 3897.
- [64b] I.A. Devyatov, M.Yu. Kupriyanov, *JETP Lett.* 77 (1993) 874.
- [65a] I.A. Devyatov, M.Yu. Kupriyanov, *Pis'ma Zh. Eksp. Teor. Fiz.* 59 (1994) 187.
- [65b] I.A. Devyatov, M.Yu. Kupriyanov, *JETP Lett.* 59 (1994) 201.
- [66] M.Yu. Kupriyanov, J.S. Tsai, *IEEE Trans. Appl. Supercond.* 5 (1995) 2531.
- [67] I.A. Devyatov, M.Yu. Kupriyanov, G. Wendin, *IEEE Trans. Appl. Supercond.* 7 (1997) 3021.
- [68] I.A. Devyatov, M.Yu. Kupriyanov, *JETP Lett.* 65 (1997) 171.
- [69a] I.A. Devyatov, M.Yu. Kupriyanov, *Zh. Eksp. Teor. Fiz.* 112 (1997) 342.
- [69b] I.A. Devyatov, M.Yu. Kupriyanov, *Sov. Phys. JETP* 86 (1997) 189.
- [70a] I.A. Devyatov, M.Yu. Kupriyanov, *Zh. Eksp. Teor. Fiz.* 114 (1998) 687.
- [70b] I.A. Devyatov, M.Yu. Kupriyanov, *Sov. Phys. JETP* 87 (1998) 375.
- [71] C.-R. Hu, *Phys. Rev. Lett.* 72 (1994) 1526.
- [72] Y. Tanaka, S. Kashiwaya, *Phys. Rev. Lett.* 74 (1995) 3451.
- [73] Yu.S. Barash, H. Burkhardt, D. Rainer, *Phys. Rev. Lett.* 77 (1996) 4070.
- [74] M. Fogelström, D. Rainer, J.A. Sauls, *Phys. Rev. Lett.* 79 (1997) 281.
- [75] L. Alff et al., *Phys. Rev. B* 55 (1997) R14757.
- [76] M. Covington, M. Aprili, L.H. Greene, F. Xu, J. Zhu, C.A. Mirkin, *Phys. Rev. Lett.* 79 (1997) 277.
- [77] M. Sigrist, K. Kuboki, P.A. Lee, A.J. Millis, T.M. Rice, *Phys. Rev. B* 53 (1996) 2835.
- [78] F.J. Culetto, G. Kieslmann, D. Rainer, in: U. Eckern, A. Schmid, W. Weber, H. Wühl (Eds.), *Proceedings of the 17th International Conference on Low Temperature Physics*, North Holland, Amsterdam, 1984, p. 1027.
- [79a] A.A. Golubov, M.Yu. Kupriyanov, *JETP Lett.* 67 (1998) 478.
- [79b] A.A. Golubov, M.Yu. Kupriyanov, *JETP Lett.* 69 (1999) 262.
- [80] L.I. Glazman, K.A. Matveev, *Sov. Phys. JETP* 67 (1988) 1276.
- [81] D.V. Goncharov, I.A. Devyatov, A.A. Golubov, M.Yu. Kupriyanov, *IEEE Trans. Appl. Supercond.* (1999) to be published.
- [82] S.P. Benz, *Appl. Phys. Lett.* 67 (1995) 2714.
- [83] H. Sachse, R. Popel, T. Weimann, F. Muller, G. Heim, J. Niemeyer, *Proc. EUCAS* 97 (1997) 555.
- [84] L. Fritzsche, M. Schubert, G. Wende, H.G. Meyer, *Appl. Phys. Lett.* 73 (1998) 1583.
- [85] T. Imamura, S. Hasio, *J. Appl. Phys.* 66 (1989) 2173.
- [86] V. Lacquaniti, S. Gonzini, S. Maggi, E. Monticoni, R. Steni, D. Andreone, *IEEE Trans. Appl. Supercond.*, ASC-98 (1999) to be published.
- [87] S.P. Benz, C.J. Burroughs, *IEEE Trans. Appl. Supercond.* 7 (1997) 2434.
- [88] C.A. Hamilton, S.P. Benz, C.J. Burroughs, T.E. Harvey, *IEEE Trans. Appl. Supercond.* 7 (1997) 2472.
- [89] K.K. Likharev, L.A. Yakobson, *Zh. Tekh. Fiz.* 45 (1973) 1503.

- [90] A.D. Zaikin, G.F. Zharkov, *Fiz. Nizk. Temp.* 7 (1981) 375.
- [91] P.N. Dmitriev, A.B. Ermakov, A.G. Kovalenko, V.P. Koshelets, N.N. Iosad, A.A. Golubov, M.Yu. Kupriyanov, *IEEE Trans. Appl. Supercond.* (1999) to be published.
- [92] A. Zehnder, Ph. Lerch, S.P. Zhao, Th. Nussbaumer, E.C. Kirk, *Phys. Rev. B* 59 (1999) 8875.
- [93] N.N. Iosad, D.V. Balashov, M.Yu. Kupriyanov, S.N. Polykov, V.V. Roddatis, *IEEE Trans. Appl. Supercond.* 7 (1997) 2808.
- [94] C.D. Thomas, M.P. Ulmer, J.B. Ketterson, *J. Appl. Phys.* 84 (1998) 364.
- [95] A.W. Kleinsasser, F.M. Rammo, M. Bushan, *Appl. Phys. Lett.* 62 (1993) 1017.
- [96] L.G. Aslamazov, A.I. Larkin, *Pis'ma Zh. Eksp. Teor. Fiz.* 9 (1969) 150.
- [97] I.O. Kulik, A.N. Omel'yanchuk, *Pis'ma Zh. Eksp. Teor. Fiz.* 21 (1975) 216.
- [98] A.A. Golubov, E.P. Houwman, J.G. Gijsbertsen, V.M. Krasnov, M.Yu. Kupriyanov, J. Floksra, H. Rogalla, *Phys. Rev. B* 51 (1995) 1073.
- [99] L.G. Aslamazov, M.V. Fistul', *Sov. Phys. JETP* 56 (1982) 666.
- [100a] A.L. Gudkov, M.Yu. Kupriyanov, K.K. Likharev, *Zh. Eksp. Teor. Fiz.* 94 (1988) 319.
- [100b] A.L. Gudkov, M.Yu. Kupriyanov, K.K. Likharev, *Sov. Phys. JETP* 68 (1988) 1478.
- [101] A. Furusaki, H. Takayanagi, M. Tsukada, *Phys. Rev. B* 45 (1992) 10563.
- [102] A. Chrestin, T. Matsuyama, U. Merkt, *Phys. Rev. B* 49 (1994) 498.
- [103] C.W.J. Beenakker, *Rev. Mod. Phys.* 69 (1997) 731.
- [104] A.A. Abrikosov, L.P. Gorkov, I.E. Dzyaloshinski, *Methods of Quantum Field Theory in Statistical Physics*, Prentice-Hall, Englewood-Cliffs, NJ, 1963.
- [105] E.N. Bratus', V.S. Shumeiko, G. Wendin, *Phys. Rev. Lett.* 74 (1995) 2110.
- [106] D.V. Averin, A. Bardas, *Phys. Rev. Lett.* 75 (1995) 1831.
- [107] A.W. Kleinsasser, R.E. Miller, W.H. Mallison, G.B. Arnold, *Phys. Rev. Lett.* 72 (1994) 1738.
- [108a] A.V. Zaitsev, *Pis'ma Zh. Eksp. Teor. Fiz.* 51 (1990) 35.
- [108b] A.V. Zaitsev, *Pis'ma JETP Lett.* 51 (1990) 41.
- [109] A.F. Volkov, A.V. Zaitsev, T.M. KLapwijk, *Physica C* 210 (1993) 21.